

An Effective Model of the Retinoic Acid Induced HL-60 Differentiation Program

Ryan Tasseff, Holly A. Jensen, Johanna Congleton[†], Wei Dai, Katherine Rogers, Adithya Sagar, Rodica P. Bunaciu[†], Andrew Yen[†], and Jeffrey D. Varner*

Robert Frederick Smith School of Chemical and Biomolecular Engineering and [†]Department of Biomedical Sciences, Cornell University, Ithaca NY 14853

Running Title: Effective modeling of HL-60 differentiation

To be submitted: ?

*Corresponding author:

Jeffrey D. Varner,

Professor, Robert Frederick Smith School of Chemical and Biomolecular Engineering,
244 Olin Hall, Cornell University, Ithaca NY, 14853

Email: jdv27@cornell.edu

Phone: (607) 255 - 4258

Fax: (607) 255 - 9166

Abstract

In this study, we present an effective model All-Trans Retinoic Acid (ATRA)-induced differentiation of HL-60 cells. The model describes a key architectural feature of ATRA-induced differentiation, positive feedback between an ATRA-inducible signalsome complex involving many proteins including Vav1, a guanine nucleotide exchange factor, and the activation of the mitogen activated protein kinase (MAPK) cascade. The model, which was developed by integrating logical rules with kinetic modeling, was significantly smaller than previous models. However, despite its simplicity, it captured key features of ATRA induced differentiation of HL-60 cells. We identified an ensemble of effective model parameters using measurements taken from ATRA-induced HL-60 cells. Using these parameters, model analysis predicted that MAPK activation was bistable as a function of ATRA exposure. Conformational experiments supported ATRA-induced bistability. These findings, combined with other literature evidence, suggest that positive feedback is central to a diversity of cell fate programs.

1 Introduction

2 Understanding the architecture of differentiation programs is an important therapeutic
3 challenge. Differentiation induction chemotherapy (DIC), using agents such as the vita-
4 min A derivative all-trans retinoic acid (ATRA), is a promising approach for the treatment
5 of many cancers (1–3). For example, ATRA treatment induces remission in 80–90% of
6 promyelocytic leukemia (APL) PML-RAR α -positive patients (4), thereby transforming a
7 fatal diagnosis into a manageable disease. However, remission is sometimes not durable
8 and relapsed cases exhibit emergent ATRA resistance (5, 6). To understand the basis of
9 this resistance, we must first understand the ATRA-induced differentiation program. To-
10 ward this challenge, lessons learned in model systems, such as the lineage-uncommitted
11 human myeloblastic cell line HL-60, could inform our analysis of the more complex dif-
12 ferentiation programs occurring in patients. Patient derived HL-60 leukemia cells have
13 been a durable experimental model since the 1970's to study differentiation (7). HL-60
14 undergoes cell cycle arrest and either myeloid or monocytic differentiation following stim-
15 ulation; ATRA induces G1/G0-arrest and myeloid differentiation in HL-60 cells, while 1,25-
16 dihydroxy vitamin D3 (D3) induces arrest and monocytic differentiation. Commitment to
17 cell cycle arrest and differentiation requires approximately 48 hr of treatment, during which
18 HL-60 cells undergo two division cycles.

19 Sustained mitogen-activated protein kinase (MAPK) activation is a defining feature of
20 ATRA-induced HL-60 differentiation. ATRA drives sustained MEK-dependent activation
21 of the Raf/MEK/ERK pathway, leading to arrest and differentiation (8). MEK inhibition re-
22 sults in the loss of ERK and Raf phosphorylation, and the failure to arrest and differentiate
23 (9). ATRA (and its metabolites) are ligands for the hormone activated nuclear transcrip-
24 tion factors retinoic acid receptor (RAR) and retinoid X receptor (RXR) (10). RAR/RXR
25 activation is necessary for ATRA-induced Raf phosphorylation (9), and the formation of
26 an ATRA-inducible signalsome complex at the membrane which drives MAPK activation

27 through a yet to be identified kinase activity. While the makeup of the signalsome com-
28 plex is not yet known, we do know that it is composed of Src family kinases Fgr and Lyn,
29 PI3K, c-Cbl, Slp76, and KSR, as well as IRF-1 transcription factors (11–15). Signalsome
30 formation and activity is driven by ATRA-induced expression of CD38 and the putative
31 heterotrimeric Gq protein-coupled receptor BLR1 (16, 17). BLR1, identified as an early
32 ATRA (or D3)-inducible gene using differential display (18), is necessary for MAPK ac-
33 tivation and differentiation (17), and is also involved with signalsome activity. Studies
34 of the BLR1 promoter identified a 5' 17bp GT box approximately 1 kb upstream of the
35 transcriptional start that conferred ATRA responsiveness (17). Members of the BLR1
36 transcriptional activator complex, e.g. NFATc3 and CREB, are phosphorylated by ERK,
37 JNK or p38 MAPK family members suggesting positive feedback between the signalsome
38 and MAPK activation (19). BLR1 overexpression enhanced Raf phosphorylation and ac-
39 celerated terminal differentiation, while Raf inhibition reduced BLR1 expression and dif-
40 ferentiation (20). BLR1 knock-out cells failed to activate Raf or differentiate in the pres-
41 ence of ATRA (20). Interestingly, both the knockdown or inhibition of Raf, also reduced
42 BLR1 expression and functional differentiation (20). Thus, the expression of signalsome
43 components e.g., BLR1 was Raf dependent, while Raf activation depended upon the sig-
44 nalsome. A previous computational study of ATRA-induced differentiation in HL-60 cells
45 suggested that the BLR1-MAPK positive feedback circuit was sufficient to explain ATRA-
46 induced sustained MAPK activation, and the expression of a limited number of functional
47 differentiation markers (21). Model analysis also suggested that Raf was the most distinct
48 of the MAPK proteins. However, this previous study developed and analyzed a complex
49 model, thus leaving open the critical question of what is the minimal positive feedback
50 circuit required to drive ATRA-induced differentiation.

51 In this study, we explored this question using a minimal mathematical model of the
52 key architectural feature of ATRA induced differentiation of HL-60 cells, namely positive

53 feedback between an ATRA-inducible signalsome complex and MAPK activation. The
54 ATRA responsive signalsome-MAPK circuit was then used to drive a downstream gene
55 expression program which encoded for the expression of intermediate and functional dif-
56 ferentiation markers. The effective model used a novel framework which integrated logi-
57 cal rules with kinetic modeling to describe gene expression and protein regulation, while
58 largely relying upon biophysical parameters from the literature. This formulation signifi-
59 cantly reduced the size and complexity of the model compared to the previous study of
60 Tasseff et al., while increasing the breadth of the biology described (21). The effective
61 model, despite its simplicity, captured key features of ATRA induced differentiation of HL-
62 60 cells. Model analysis predicted the bistability of MAPK activation as a function of ATRA
63 exposure; conformational experiments supported ATRA-induced bistability. Model simu-
64 lations were also consistent with measurements of the influence of MAPK inhibitors, and
65 the failure of BLR1 knockout cells to differentiate when exposed to ATRA. In addition, the
66 expression of intermediate and phenotypic differentiation markers as also captured follow-
67 ing ATRA exposure. Lastly, we showed by through immunoprecipitation studies, that the
68 guanine nucleotide exchange factor Vav1 is potentially a new ATRA-inducible member of
69 the signalsome complex. Taken together, these findings when combined with other litera-
70 ture evidence, suggested that positive feedback architectures are central to differentiation
71 programs generally, and necessary for ATRA-induced differentiation.

72 **Results**

73 We constructed an effective model of ATRA-induced HL-60 differentiation which described
74 signaling and gene expression events following the addition of ATRA (Fig. 1). The model
75 connectivity was developed from literature and the studies presented here (Table 1). We
76 decomposed the ATRA program into three modules; a signal initiation module that sensed
77 and transformed the ATRA signal into activated cRaf-pS621 and the ATRA-RXR/RAR
78 (Trigger) signals (Fig. 1A); a signal integration module that controlled the expression of
79 upstream transcription factors given cRaf-pS621 and activated Trigger signals (Fig. 1B);
80 and a phenotype module which encoded the expression of functional differentiation mark-
81 ers from the ATRA-inducible transcription factors (Fig. 1C). Each component of these
82 modules was described by a mRNA and protein balance equation. Additionally, the sig-
83 nal initiation module also described the abundance of activated species e.g., Trigger and
84 cRaf-pS621 whose values were derived from unactivated Trigger and cRaf protein levels.
85 Lastly, because the population of HL-60 cells was dividing (at least before ATRA-induced
86 cell cycle arrest), we also considered a dilution term in all balance equations. The sig-
87 nal initiation module contained nine differential equations, while the signal integration and
88 phenotype modules were collectively encoded by 54 differential equations. Model param-
89 eters were taken literature (Table 2), or estimated from experimental data using heuristic
90 optimization (see materials and methods).

91 The signal initiation module recapitulated sustained signalsome and MAPK activation
92 following exposure to $1\mu\text{M}$ ATRA (Fig. 2A-B). An ensemble of effective model param-
93 eters was estimated by minimizing the difference between simulations and time-series
94 measurements of BLR1 mRNA and cRaf-pS621 following the addition of $1\mu\text{M}$ ATRA. We
95 focused on the S621 phosphorylation site of cRaf since enhanced phosphorylation at
96 this site is a defining characteristic of sustained MAPK activation in HL-60. The effective
97 model captured both ATRA-induced BLR1 expression (Fig. 2A) and sustained phospho-

98 phosphorylation of cRaf-pS621 (Fig. 2B) in a growing population of HL-60 cells. Together, the
99 reinforcing positive feedback between the signalsome and MAPK led to sustained activation
100 over multiple cellular generations. However, the effective model failed to capture the
101 decline of BLR1 message after 48 hr of ATRA exposure. This suggested that we captured
102 the logic leading to the onset of differentiation, but failed to describe program shutdown.
103 Next, we tested the response of the signal initiation module to different ATRA dosages.

104 The signal initiation model was bistable with respect to ATRA induction (Fig. 2C-D).
105 Phaseplane analysis predicted two stable steady-states when ATRA was present below
106 a critical threshold, and only a single steady-state above the threshold (Fig. 2C). In the
107 lower stable state, neither the signalsome nor cRaf-pS621 were present (thus, the differ-
108 entiation program was deactivated). However, at the high stable state, both the signal-
109 some and cRaf-pS621 were present, allowing for sustained activation and differentiation.
110 Interestingly, when ATRA was above a critical threshold, only the activated state was ac-
111 cessible (Fig. 2D). To test these findings, we first identified the ATRA threshold. We
112 exposed HL-60 cells to different ATRA concentrations for 72 hr (Fig. 2E). Morphological
113 changes associated with differentiation were visible for ATRA \geq 0.25 μ M, suggesting the
114 critical ATRA threshold was near this concentration. Next, we conducted ATRA washout
115 experiments to determine if activated cells remained activated in the absence of ATRA.
116 HL-60 cells locked into an activated state remained activated following ATRA withdraw-
117 (Fig. 3). This sustained activation resulted from reinforcing feedback between the sig-
118 nalsome and the MAPK pathway. Thus, following activation, if we inhibited or removed
119 elements from the signal initiation module we expected the signalsome and MAPK signals
120 to decay. We simulated ATRA induced activation in the presence of kinase inhibitors, and
121 without key circuit elements. Consistent with experimental results using multiple MAPK
122 inhibitors, ATRA activation in the presence of MAPK inhibitors lowered the steady-state
123 value of signalsome (Fig. 3A). In the presence of BLR1, the signalsome and cRaf-pS621

signals were maintained following ATRA withdraw (Fig. 3B, gray). On the other hand, BLR1 deletion removed the ability of the circuit to maintain a sustained MAPK response following the withdraw of ATRA (Fig. 3B, blue). Lastly, washout experiments in which cells were exposed to $1\mu\text{M}$ ATRA for 24 hr, and then transferred to fresh media without ATRA, confirmed the persistence of the self sustaining activated state for up to 144 hr (Fig. 3C). Thus, these experiments confirmed that reinforcing positive feedback likely drives the ATRA-induced differentiation program. Next, we analyzed the ATRA-induced downstream gene expression program following signalsome and cRaf activation.

The signal integration and phenotype modules described ATRA-induced gene expression in wild-type HL-60 cells (Fig. 4). The signal initiation module produced two outputs, activated Trigger and cRaf-pS621 which drove the expression of ATRA-induced transcription factors, which then in turn activated the phenotypic program. In particular, Trigger (a surrogate for the RAR α /RXR transcriptional complex) regulated the expression of the transcription factors CCATT/enhancer binding protein α (C/EBP α), PU.1, and Egr-1. In turn, these transcription factors, in combination with cRaf-pS621, regulated the expression of downstream phenotypic markers such as CD38, CD11b or p47Phox. We assembled the connectivity of the signal integration and phenotypic programs driven by Trigger and cRaf-pS621 from literature (Table 1). We estimated the parameters for the signal initiation, and phenotype modules from steady-state and dynamic measurements of transcription factor and phenotypic marker expression following the addition of ATRA (22–25). However, the bulk of the model parameters were taken from directly from literature (26) and were not estimated in this study (see materials and methods). The model simulations captured the time dependent expression of CD38 and CD11b following the addition ATRA (Fig. 4A), and the steady-state for signal integration and phenotypic markers (Fig. 4B). Lastly, we used the *predicted* values of the p21 and E2F protein abundance to estimate a black-box model of ATRA-induced G0 arrest (Fig. 5). The phenotype module predicted p21

expression significantly increased and E2F expression decreased, in response to ATRA exposure (Fig. 5A). We then used the ratio of these values in a polynomial model to calculate the fraction of HL-60 cells in G0 arrest following the addition of ATRA (Fig. 5B). The third-order polynomial model captured the trend in measured G0-arrest values as a function of time, and was robust to uncertainty in the measured data (Fig. 5B, gray). Taken together, the output of the signal integration and phenotypic modules was consistent with time-series and steady-state measurements, thereby validating the assumed molecular connectivity. Moreover, outputs from the phenotype module described the trend in ATRA-induced G0 cell cycle arrest. Next, we explored which nodes and interactions between nodes in the signal integration module most influenced the system response.

The Gfi-1 and PPAR γ proteins were important regulators of ATRA-induced signal integration and phenotypic change (Fig. 6). We conducted pairwise gene knockout simulations in the signal integration and phenotype modules to estimate which nodes controlled the processing of the Trigger and cRaF-S621 signals. The difference between the system state with and without the gene knockouts (encoded as a normalized state displacement matrix) was decomposed using Singular Value Decomposition (SVD). A panel of ten parameter sets was sampled, and the average normalized displacement matrix was decomposed. The first six modes (approximately 36% of the total) described >95% of the gene knockout variance, with the most important components of these modes being the Gfi-1 and PPAR γ proteins, and to a lesser extent PU.1, C/EBP α and AP1 (Fig. 6A). To better understand which protein-DNA connections were important, we simulated the pairwise deletion of interactions between these proteins and their respective regulatory targets. SVD decomposition of the normalized state displacement matrix assembled from the pairwise connection deletions, suggested the first six modes (approximately 26% of the total) accounted for >90% of the variance. Globally, the most sensitive interactions controlled p21 and p47Phox expression, markers for cell-cycle arrest and reactive oxygen

176 formation phenotypic axes activated following ATRA addition (Fig. 6B). Analysis of the
177 modes suggested the action of PPARg, Gfi-1 and C/EBPa were consistently important
178 over multiple target genes. The connection knockout analysis also revealed robustness
179 in the network. For example, no pair of deletions qualitatively changed the expression of
180 regulators such as PU.1, Oct1, Oct4 or PPARg. Thus, the expression of these species
181 was robust to disturbance in the connectivity. To better understand the combined influ-
182 ence of the PPARg and Gfi-1 deletions, we computed the fold change in the protein levels
183 in the single ($Gfi-1^{-/-}$ or $PPARg^{-/-}$) and double ($Gfi-1^{-/-}$ and $PPARg^{-/-}$) mutants for
184 the best fit parameter set (Fig. 7). Deletion of Gfi-1 led to a 2-4 fold increase in EGR-1,
185 CD11b and C/EBPa expression, and a >8 fold increase in PU.1 abundance (Fig. 7,blue).
186 On the other hand, deletion of PPARg led to >8 fold downregulation of CD38, p21, IRF1
187 and OCT1 (Fig. 7,red). Both knockouts slightly increased E2F expression, but neither
188 influenced the expression of p47Phox. The double mutant was qualitatively similar to the
189 combined behavior of the two single mutant cases. Taken together, Gfi-1 and PPARg
190 controlled the cell-cycle arrest and receptor signaling axes, with PPARg regulating CD38,
191 IRF1 and p21 expression while Gfi-1 controlled CD11b expression. These simulations
192 suggested deletion of PPARg and Gfi-1 would not interfere with reactive oxygen forma-
193 tion, but would limit the ability of HL-60 cells to arrest. However, this analysis did not
194 give insight into which components upstream of the signal initiation module were impor-
195 tant. Toward this question, we explored the composition and regulation of the signalsome
196 complex by experimentally interrogating a panel of possible Raf interaction partners.

197 The composition of the signalsome, and the kinase ultimately responsible for medi-
198 ating ATRA-induced Raf activation is currently unknown. To explore this question, we
199 conducted immunoprecipitation and subsequent Western blotting to identify physical in-
200 teractions between Raf and 19 putative interaction partners. A panel of 19 possible Raf
201 interaction partners (kinases, GTPases, scaffolding proteins etc) was constructed based

upon known signaling pathways. We did not consider the most likely binding partner, the small GTPase RAS, as previous studies have ruled it out in MAPK activation in HL-60 cells (20, 27). Total Raf was used as a bait protein for the immunoprecipitation studies. Interrogation of the Raf interactome suggested Vav1 was involved with ATRA-induced initiation of MAPK activity (Fig. 8). Western blot analysis using total Raf and pS621 Raf specific antibodies confirmed the presence of the bait protein, total and phosphorylated forms, in the immunoprecipitate (Fig. 8A). Of the 19 proteins sampled, Vav1, Src, CK2, Akt, and 14-3-3 precipitated with Raf, suggesting a direct physical interaction was possible. However, only the associations between Raf and Vav1 and Raf and Src were ATRA-inducible (Fig. 8). Furthermore, the Vav1 and Src associations were correlated with pS621 Raf abundance in the precipitate. Others proteins e.g., CK2, Akt and 14-3-3, generally bound Raf regardless of phosphorylation status or ATRA treatment. The remaining 14 proteins were expressed in whole cell lysate (Fig. 8B), but were not detectable in the precipitate of Raf IP. Treatment with the Raf kinase inhibitor GW5074 following ATRA exposure reduced the association of both Vav1 with Raf and Src with Raf (Fig. 8), although the signal intensity for Src was notably weak. However, GW5074 did not influence the association of CK2 or 14-3-3 with Raf, further demonstrating their independence from Raf phosphorylation. Interestingly, the Raf-Akt interaction qualitatively increased following treatment with GW5074; however, it remained unaffected by treatment with ATRA. Src family kinases are known to be important in myeloid differentiation (28) and their role in HL-60 differentiation has been investigated elsewhere (11). Given the existing work and variable reproducibility in the context of the Raf immunoprecipitate, we did not investigate the role of Src further in this study. Taken together, the immunoprecipitation and GW5074 results implicated Vav1 association to be correlated with Raf activation following ATRA-treatment. Previous studies demonstrated that a Vav1-Slp76-Cbl-CD38 complex plays an important role in ATRA-induced MAPK activation and differentiation of HL-60 cells (13). Here we

228 did not observe direct interaction of Raf with Cbl or Slp76; however, this complex could
229 be involved upstream. Next, we considered the effect of the Raf kinase inhibitor GW5074
230 on functional markers of ATRA-induced growth arrest and differentiation.

231 Inhibition of Raf kinase activity modulated MAPK activation and differentiation mark-
232 ers following ATRA exposure (Fig. 8D-F). ATRA treatment alone statistically significantly
233 increased the G1/G0 percentage over the untreated control, while GW5074 alone had a
234 negligible effect on the cell cycle distribution (Fig. 8D). Surprisingly, the combination of
235 GW5074 and ATRA statistically significantly increased the G1/G0 population ($82 \pm 1\%$)
236 compared with ATRA alone ($61 \pm 0.5\%$). Increased G1/G0 arrest following the combined
237 treatment with GW5074 and ATRA was unexpected, as the combination of ATRA and the
238 MEK inhibitor (PD98059) has been shown previously to decrease ATRA-induced growth
239 arrest (8). However, growth arrest is not the sole indication of functional differentiation.
240 Expression of the cell surface marker CD11b has also been shown to coincide with HL-60
241 cells myeloid differentiation (29). We measured CD11b expression, for the various treat-
242 ment groups, using immuno-fluorescence flow cytometry 48 hr post-treatment. As with
243 G1/G0 arrest, ATRA alone increased CD11b expression over the untreated control, while
244 GW5074 further enhanced ATRA-induced CD11b expression (Fig. 8E). GW5074 alone
245 had no statistically significant effect on CD11b expression, compared with the untreated
246 control. Lastly, the inducible reactive oxygen species (ROS) response was used as a func-
247 tional marker of differentiated neutrophils (16). We measured the ROS response induced
248 by the phorbol ester 12-O-tetradecanoylphorbol-13-acetate (TPA) using flow cytometry.
249 Untreated cells showed no discernible TPA response, with only $7.0 \pm 3.0\%$ ROS induction
250 (Fig. 8F). Cells treated with ATRA had a significantly increased TPA response, $53 \pm 7\%$
251 ROS induction 48 hr post-treatment. Treatment with both ATRA and GW5074 statistically
252 significantly reduced ROS induction ($22 \pm 0.6\%$) compared to ATRA alone. Interestingly,
253 Western blot analysis did not detect a GW5074 effect on ATRA-induced expression of

²⁵⁴ p47Phox, a required upstream component of the ROS response (Fig. 8F, bottom). Thus,
²⁵⁵ the inhibitory effect of GW5074 on inducible ROS might occur downstream of p47Phox
²⁵⁶ expression. However, the ROS producing complex is MAPK dependent, therefore it is
²⁵⁷ also possible that GW5074 inhibited ROS production by interfering with MAPK activation
²⁵⁸ (in which case the p47Phox marker might not accurately reflect phenotypic conversion
²⁵⁹ and differentiation).

260 **Discussion**

261 In this study, we presented an effective model of ATRA-inducible differentiation of HL-60
262 cells. The model consisted of three modules: a signal initiation module that sensed and
263 transformed the ATRA signal into activated cRaf-pS621 and the ATRA-RXR/RAR (Trig-
264 ger) signals; a signal integration module that controlled the expression of upstream tran-
265 scription factors given cRaf-pS621 and activated Trigger signals; and a phenotype mod-
266 ule which encoded the expression of functional differentiation markers from the ATRA-
267 inducible transcription factors. The model described the transcription and translation of
268 genes in each module, and signaling events in each module in a growing population of
269 HL-60 cells. Model parameters were taken from literature, however, unknown coefficients
270 that appear in the promoter logic models were estimated from protein measurements in
271 HL-60 cells following ATRA exposure. Despite its simplicity, the effective model captured
272 key features of the ATRA induced differentiation such as sustained MAPK activation, and
273 bistability with respect to ATRA exposure. The model also described the expression of
274 upstream transcription factors which regulated the expression of differentiation markers.
275 Lastly, analysis of the response of the model to perturbations identified Gfi-1 and PPARg
276 as master regulators of ATRA-induced differentiation. We also reported a new ATRA-
277 inducible component of the signalsome, Vav1. Vav1 is a guanine nucleotide exchange
278 factor for Rho family GTPases that activate pathways leading to actin cytoskeletal re-
279 arrangements and transcriptional alterations (30). The Vav1/Raf association correlated
280 with Raf activity, was ATRA-inducible and decreased after treatment with the Raf inhibitor
281 GW5074.

282 Naturally occurring cell fate decisions often incorporate reinforcing feedback and bista-
283 bility (31, 32). One of the most well studied cell fate circuits is the Mos mitogen-activated
284 protein kinase cascade in *Xenopus* oocytes. This cascade is activated when oocytes are
285 induced by the steroid hormone progesterone (33). The MEK-dependent activation of

286 p42 MAPK stimulates the accumulation of the Mos oncoprotein, which in turn activates
287 MEK, thereby closing the feedback loop. This is similar to the signal initiation module
288 presented here; ATRA drives signalsome formation, which activates MAPK, which in turn
289 leads to more signalsome activation. Thus, while HL-60 and *Xenopus* oocytes are vastly
290 different biological models, their cell fate programs share a similar architectural feature.
291 Reinforcing feedback and bistability has also been implicated in hematopoietic cell fate
292 determination. Laslo et al showed that the counter antagonistic repressors, Gfi-1 and
293 Egr-1/2 (whose expression is tuned by PU.1 and C/EBPa), encodes a bistable switch that
294 results in a macrophage, neutrophil or a mixed lineage population depending upon PU.1
295 and C/EBPa expression (32). The current model contained the Gfi-1 and Egr-1/2 agonis-
296 tic switch; however, its significance was unclear for HL-60 cells. The expression of Gfi-1,
297 Egr-1/2, C/EBPa and PU.1 was not consistent with the canonical lineage pattern expected
298 from literature. For example, Egr-1/2 expression (associated with a macrophage lineage)
299 increased, while Gfi-1 expression (associated with a neutrophil lineage) remained con-
300 stant following ATRA exposure. Literature evidence in nonmalignant myelomonocytic fate
301 selection has shown that Gfi-1 and Egr-1/2 promote granulocytic and monocytic differ-
302 entiation, respectively (32). Thus, HL-60 cells, which are a less mature cancer cell line,
303 exhibited a non-canonical expression pattern. Other unrelated cell fate decisions such
304 as programmed cell death have also been suggested to be bistable (34). Still more bio-
305 chemical networks important to human health, for example the human coagulation or
306 complement cascades, also feature strong positive feedback elements (35). Thus, while
307 reinforcing feedback is often undesirable in human engineered systems, it is at the core
308 of a diverse variety of cell fate programs and other networks important to human health.

309 Analysis of the signal integration and phenotype modules suggested that Gfi-1 and
310 PPAR γ were required for ATRA-induced differentiation in HL-60 cells. Model analysis
311 showed that PU.1, Egr-1 and C/EBPa expression increased in Gfi-1 $^{-/-}$ mutants, where

312 PU.1 expression was upregulated by greater than 8-fold. PU.1, a member of the *ets* trans-
313 scription factor family, is a well known regulator of granulocyte and monocyte development
314 (36). The relative level of PU.1 and C/EBPa is thought to control macrophage versus neu-
315 trophil cell fate decisions in granulocytic macrophage progenitor cells (37). Simulations
316 suggested that combined Gfi-1 + PPARg deletion crippled the ability of HL-60 cells to
317 undergo neutrophilic differentiation following ATRA exposure. p21 expression decreased
318 significantly, suggesting Gfi-1^{-/-} + PPARg^{-/-} mutants were less likely to G0-arrest fol-
319 lowing ATRA exposure. The expression of other neutrophilic markers, such as CD38,
320 also decreased in Gfi-1^{-/-} + PPARg^{-/-} cells. On the other hand, the expression of re-
321 active oxygen metabolic markers, or other important transcription factors such as OCT4
322 did not change. For example, model analysis suggested that the C/EBPa dependent in-
323 teraction of PU.1 with the *NCF1* gene, which encodes the p47Phox protein, was the most
324 sensitive PU.1 connection; deletion of this connection removed the ability of the system
325 to express p47Phox. p47Phox, also known as neutrophil cytosol factor 1, is one of four
326 cytosolic subunits of the multi-protein NADPH oxidase complex found in neutrophils (38).
327 This enzyme is responsible for reactive oxygen species (ROS) production, a key compo-
328 nent of the anti-microbial function of neutrophils. However, Gfi-1 deletion did not increase
329 p47Phox expression, nor did the deletion of PPARg. This suggested that while p47Phox
330 expression required C/EBPa and PU.1, it was saturated with respect these proteins, and
331 simultaneously not sensitive to PPARg abundance. Together, Gfi-1^{-/-} + PPARg^{-/-} cells
332 were predicted to exhibit some aspects of the ATRA response, but not other critical fea-
333 tures such as cell cycle arrest. Hock et al showed that Gfi-1^{-/-} mice lacked normal
334 neutrophils, and were highly sensitive to bacterial infection (39). Thus, the model analysis
335 was consistent with this study. However, other predictions concerning the behavior of the
336 Gfi-1^{-/-} + PPARg^{-/-} mutants have yet to be verified experimentally.

337 Immunoprecipitation studies identified a limited number of ATRA-dependent and -

338 independent Raf interaction partners. While we were unable to detect the association
339 of Raf with common kinases and GTPases such as PKC, PKA, p38, Rac and Rho, we
340 did establish potential interactions between Raf and key partners such as Vav1, Src, Akt,
341 CK2 and 14-3-3. All of these partners are known to be associated with Raf activation
342 or function. Src is known to bind Raf through an SH2 domain, and this association has
343 been shown to be dependent of the serine phosphorylation of Raf (40). Thus, an ATRA in-
344 ducible Src/Raf association may be a result of ATRA-induced Raf phosphorylation at S259
345 or S621. We also identified an interaction between Raf and the Ser/Thr kinases Akt and
346 CK2. Akt can phosphorylate Raf at S259, as demonstrated by studies in a human breast
347 cancer line (41). CK2 can also phosphorylate Raf, although the literature has traditionally
348 focused on S338 and not S621 or S259(42). However, neither of these kinase interactions
349 were ATRA-inducible, suggesting their association with Raf alone was not associated with
350 ATRA-induced Raf phosphorylation. The adapter protein 14-3-3 was also constitutively
351 associated with Raf. The interaction between Raf and 14-3-3 has been associated with
352 both S621 and S259 phosphorylation and activity (43). Additionally, the association of
353 Raf with 14-3-3 not only stabilized S621 phosphorylation, but also reversed the S621
354 phosphorylation from inhibitory to activating (44). Finally, we found that Vav1/Raf associ-
355 ation correlated with Raf activity, was ATRA-inducible and decreased after treatment with
356 GW5074. The presence of Vav1 in Raf/Grb2 complexes has been shown to correlate with
357 increased Raf activity in mast cells (45). Furthermore, studies on Vav1 knockout mice
358 demonstrated that the loss of Vav1 resulted in deficiencies of ERK signaling for both T-
359 cells as well as neutrophils (46, 47). Interestingly, while an integrin ligand-induced ROS
360 response was blocked in Vav1 knockout neutrophils, TPA was able to bypass the Vav1
361 requirement and stimulate both ERK phosphorylation and ROS induction (47). In this
362 study, the TPA-induced ROS response was dependent upon Raf kinase activity, and was
363 mitigated by the addition of GW5074. It is possible that Vav1 is downstream of various

364 integrin receptors but upstream of Raf in terms of inducible ROS responses. Vav1 has
365 also been shown to associate with a Cbl-Slp76-CD38 complex in an ATRA-dependent
366 manner; furthermore, transfection of HL-60 cells with Cbl mutants that fail to bind CD38,
367 yet still bind Slp76 and Vav1, prevents ATRA-induced MAPK activation (13). The literature
368 suggest a variety of possible receptor-signaling pathways, which involve Vav1, for MAPK
369 activation; moreover, given the ATRA-inducible association Vav1 may play a direct role in
370 Raf activation.

371 We hypothesized that Vav1 is a member of an ATRA-inducible complex which propels
372 sustained MAPK activation, arrest and differentiation. Initially, ATRA-induced Vav1 ex-
373 pression drives increased association between Vav1 and Raf. This increased interaction
374 facilitates phosphorylation and activation of Raf by pre-bound Akt and/or CK2 at S621
375 or perhaps S259. Constitutively bound 14-3-3 may also stabilize the S621 phosphory-
376 lation, modulate the activity and/or up-regulate autophosphorylation. Activated Raf can
377 then drive ERK activation, which in turn closes the positive feedback loop by activating
378 Raf transcription factors e.g., Sp1 and/or STAT1 (48–51). We tested this working hy-
379 pothesis using mathematical modeling. The model recapitulated both ATRA time-course
380 data as well as the GW5074 inhibitor effects. This suggested the proposed Raf-Vav1
381 architecture was at least consistent with the experimental studies. Further, analysis of
382 the Raf-Vav1 model identified bistability in ppERK levels. Thus, two possible MAPK ac-
383 tivation branches were possible for experimentally testable ATRA values. The analysis
384 also suggested the ATRA-induced Raf-Vav1 architecture could be locked into a sustained
385 signaling mode (high ppERK) even in the absence of a ATRA signal. This locked-in prop-
386 erty could give rise to an ATRA-induction memory. We validated the treatment memory
387 property predicted by the Raf-Vav1 circuit experimentally using ATRA-washout experi-
388 ments. ERK phosphorylation levels remained high for more than 96 hr after ATRA was
389 removed. Previous studies demonstrated that HL-60 cells possessed an inheritable mem-

390 ory of ATRA stimulus (52). Although the active state was self-sustaining, the inactive state
391 demonstrated considerable robustness to perturbation. For example, we found that 50x
392 overexpression of Raf was required to reliably lock MAPK into the activated state, while
393 small perturbations had almost no effect on ppERK levels over the entire ensemble. CD38
394 expression correlated with the ppERK, suggesting its involvement in the signaling com-
395 plex. Our computational and experimental results showed that positive feedback, through
396 ERK-dependent Raf expression, could sustain MAPK signaling through many division cy-
397 cles. Such molecular mechanisms could underly aspects of cellular memory associated
398 to consecutive ATRA treatments.

399 **Materials and Methods**

400 *Effective gene expression model equations.* We decomposed the ATRA-induced differ-
 401 entiation program into three modules; a signal initiation module that sensed and trans-
 402 formed the ATRA signal into activated cRaf-pS621 and the ATRA-RXR/RAR (activated
 403 Trigger) signals; a signal integration module that controlled the expression of upstream
 404 transcription factors given cRaf-pS621 and activated Trigger signals; and a phenotype
 405 module which encoded the expression of functional differentiation markers from the ATRA-
 406 inducible transcription factors. The output of the signal initiation module was the input to
 407 the gene expression model. For each gene $j = 1, 2, \dots, \mathcal{G}$, we modeled both the mRNA
 408 (m_j), protein (p_j) and signaling species abundance:

$$\frac{dm_j}{dt} = r_{T,j} - (\mu + \theta_{m,j}) m_j + \lambda_j \quad (1)$$

$$\frac{dp_j}{dt} = r_{X,j} - (\mu + \theta_{p,j}) p_j \quad (2)$$

$$g(p_1, \dots, p_{\mathcal{G}}, \kappa) = 0 \quad (3)$$

409 The terms $r_{T,j}$ and $r_{X,j}$ denote the specific rates of transcription, and translation while
 410 the terms $\theta_{m,j}$ and $\theta_{p,j}$ denote first-order degradation constants for mRNA and protein,
 411 respectively. The specific transcription rate $r_{T,j}$ was modeled as the product of a kinetic
 412 term $\bar{r}_{T,j}$ and a control term u_j which described how the abundance of transcription fac-
 413 tors, or other regulators influenced the expression of gene j . The kinetic transcription
 414 term $\bar{r}_{T,j}$ was modeled as:

$$\bar{r}_{T,j} = V_T^{max} \left(\frac{L_{T,o}}{L_{T,j}} \right) \left(\frac{G_j}{K_T + G_j} \right) \quad (4)$$

415 where the maximum gene expression rate V_T^{max} was defined as the product of a char-
 416 acteristic transcription rate constant (k_T) and the abundance of RNA polymerase (R_1),

417 $V_T^{max} = k_T(R_1)$. The $(L_{T,o}/L_{T,j})$ term denotes the ratio of transcription read lengths; $L_{T,o}$
 418 represents a characteristic gene length, while $L_{T,j}$ denotes the length of gene j . Thus,
 419 the ratio $(L_{T,o}/L_{T,j})$ is a gene specific correction to the characteristic transcription rate
 420 V_T^{max} . The degradation rate constants were defined as $\theta_{m,j}$ and $\theta_{p,j}$ denote characteristic
 421 degradation constants for mRNA and protein, respectively. Lastly, the λ_j term denotes the
 422 constitutive rate of expression of gene j .

423 The gene expression control term $0 \leq u_j \leq 1$ depended upon the combination of fac-
 424 tors which influenced the expression of gene j . If the expression of gene j was influenced
 425 by $1, \dots, m$ factors, we modeled this relationship as $u_j = \mathcal{I}_j(f_{1j}(\cdot), \dots, f_{mj}(\cdot))$ where
 426 $0 \leq f_{ij}(\cdot) \leq 1$ denotes a regulatory transfer function quantifying the influence of factor i
 427 on the expression of gene j , and $\mathcal{I}_j(\cdot)$ denotes an integration rule which combines the
 428 individual regulatory inputs for gene j into a single control term. In this study, the integra-
 429 tion rule governing gene expression was the weighted fraction of promoter configurations
 430 that resulted in gene expression (53):

$$u_j = \frac{W_{R_{1,j}} + \sum_n W_{nj} f_{nj}}{1 + W_{R_{1,j}} + \sum_d W_{dj} f_{dj}} \quad (5)$$

431 The numerator, the weighted sum (with weights W_{nj}) of promoter configurations leading to
 432 gene expression, was normalized by all possible promoter configurations. The likelihood
 433 of each configuration was quantified by the transfer function f_{nj} (which we modeled using
 434 hill like functions), while the lead term in the numerator $W_{R_{1,j}}$ denotes the weight of con-
 435 stitutive expression for gene j . Given this formulation, the rate of constitutive expression
 436 was then given by:

$$\lambda_j = \bar{r}_{T,j} \left(\frac{W_{R_{1,j}}}{1 + W_{R_{1,j}}} \right) \quad (6)$$

437 If a gene expression process had no modifying factors, $u_j = 1$. Lastly, the specific trans-

438 lation rate was modeled as:

$$r_{X,j} = V_X^{\max} \left(\frac{L_{X,o}}{L_{X,j}} \right) \left(\frac{m_j}{K_X + m_j} \right) \quad (7)$$

439 where V_X^{\max} denotes a characteristic maximum translation rate estimated from literature,
440 and K_X denotes a translation saturation constant. The characteristic maximum translation
441 rate was defined as the product of a characteristic translation rate constant (k_X) and
442 the Ribosome abundance (R_2), $V_X^{\max} = k_X (R_2)$. As was the case for transcription, we
443 corrected the characteristic translation rate by the ratio of the length of a characteristic
444 transcription normalized by the length of transcript j .

445 *Signaling model equations.* The signal initiation, and integration modules required the
446 abundance of cRaf-pS621 and ATRA-RXR/RAR (activated Trigger) as inputs. However,
447 our base model described only the abundance of inactive proteins e.g., cRaf or RXR/RAR
448 but not the activated forms. To address this issue, we estimated pseudo steady state
449 approximations for the abundance of cRaf-pS621 and activated Trigger (shown generally
450 as Eq (3)). The abundance of activated trigger ($x_{a,1}$) was estimated directly from the
451 RXR/RAR abundance ($x_{u,1}$):

$$x_{a,1} \sim x_{u,1} \left(\frac{\alpha \cdot \text{ATRA}}{1 + \alpha \cdot \text{ATRA}} \right) \quad (8)$$

452 where α denotes a gain parameter; $\alpha = 0.0$ if ATRA is less than a threshold, and $\alpha = 0.1$
453 if ATRA is greater than the differentiation threshold. The abundance of cRaf-pS621 was
454 estimated by making the pseudo steady state approximation on the cRaf-pS621 balance.
455 The abundance of an activated signaling species i was given by:

$$\frac{dx_i}{dt} = r_{+,i}(\mathbf{x}, \mathbf{k}) - (\mu + k_{d,i}) x_i \quad i = 1, \dots, \mathcal{M} \quad (9)$$

456 The quantity x_i denotes concentration of signaling species i , while \mathcal{R} and \mathcal{M} denote
 457 the number of signaling reactions and signaling species in the model, respectively. The
 458 term $r_{+,i}(\mathbf{x}, \mathbf{k})$ denotes the rate of generation of activated species i , while μ denotes
 459 the specific growth rate, and $k_{d,i}$ denotes the rate constant controlling the non-specific
 460 degradation of x_i . We neglected deactivation reactions e.g., phosphatase activities. We
 461 assumed that signaling processes were fast compared to gene expression; this allowed
 462 us to approximate the signaling balance as:

$$x_i^* \simeq \frac{r_{+,i}(\mathbf{x}, \mathbf{k})}{(\mu + k_{d,i})} \quad i = 1, \dots, \mathcal{M} \quad (10)$$

463 The generation rate was written as the product of a kinetic term ($\bar{r}_{+,i}$) and a control term
 464 (v_i). The control terms $0 \leq v_j \leq 1$ depended upon the combination of factors which in-
 465 fluenced rate process j . If rate j was influenced by $1, \dots, m$ factors, we modeled this
 466 relationship as $v_j = \mathcal{I}_j(f_{1j}(\cdot), \dots, f_{mj}(\cdot))$ where $0 \leq f_{ij}(\cdot) \leq 1$ denotes a regulatory
 467 transfer function quantifying the influence of factor i on rate j . The function $\mathcal{I}_j(\cdot)$ is an
 468 integration rule which maps the output of regulatory transfer functions into a control vari-
 469 able. In this study, we used $\mathcal{I}_j \in \{\min, \max\}$ and hill transfer functions (54). If a process
 470 had no modifying factors, $v_j = 1$. The kinetic rate of cRaf-pS621 generation $\bar{r}_{+,cRaf}$ was
 471 modeled as:

$$\bar{r}_{+,cRaf} = k_{+,cRaf} x_s \left(\frac{x_{cRaf}}{K_{+,cRaf} + x_{cRaf}} \right) \quad (11)$$

472 where x_s denotes the signalsome abundance, and $K_{+,cRaf}$ denotes a saturation constant
 473 governing cRaf-pS621 formation. The formation of cRaf-pS621 was regulated by only a
 474 single factor, the abundance of MAPK inhibitor, thus $v_{+,cRaf}$ took the form:

$$v_{+,cRaf} = \left(1 - \frac{I}{K_D + I} \right) \quad (12)$$

475 where I denotes the abundance of the MAPK inhibitor, and K_D denotes the inhibitor
476 affinity.

477 *Estimation of gene expression model parameters.* We estimated parameters appearing
478 in the mRNA and protein balances, the abundance of polymerases and ribosomes, tran-
479 scription and translation rates, the half-life of a typical mRNA and protein, and typical
480 values for the copies per cell of RNA polymerase and ribosomes from literature (Table 2).
481 The saturation constants K_X and K_T were adjusted so that gene expression and trans-
482 lation resulted in gene products on a biologically realistic concentration scale. Lastly, we
483 calculated the concentration for gene G_j by assuming, on average, that a cell had two
484 copies of each gene at any given time. Thus, the bulk of our gene expression model pa-
485 rameters were based directly upon literature values, and were not adjusted during model
486 identification. However, the remaining parameters, e.g., the W_{ij} appearing in the gene
487 expression control laws, or parameters appearing in the transfer functions f_{dij} , were esti-
488 mated from the protein expression and signaling data sets discussed here.

489 Signaling and gene expression model parameters were estimated by minimizing the
490 squared difference between simulations and experimental protein data set j . We mea-
491 sured the squared difference in the scale, fold change and shape for protein j :

$$E_j(\mathbf{k}) = \left(\mathcal{M}_j(t_-) - \hat{y}_j(t_-, \mathbf{k}) \right)^2 + \sum_{i=1}^{\mathcal{T}_j} \left(\hat{\mathcal{M}}_{ij} - \hat{y}_{ij}(\mathbf{k}) \right)^2 + \sum_{i=1}^{\mathcal{T}_j} \left(\mathcal{M}'_{ij} - y'_{ij}(\mathbf{k}) \right)^2 \quad (13)$$

492 The first term in Eqn. (13) quantified the initial *scale* error, directly before the addition
493 of ATRA. In this case, $\mathcal{M}_j(t_-)$ (the approximate concentration of protein j before the
494 addition of ATRA) was estimated from literature. This term was required because the
495 protein measurements were reported as the fold-change; thus, the data was normalized
496 by a control value measured before the addition of ATRA. However, the model operated on
497 a physical scale. The first term allowed the model to capture physically realistic changes

498 following ATRA addition. The second term quantified the difference in the *fold-change* of
 499 protein j as a function of time. The terms $\hat{\mathcal{M}}_{ij}$ and \hat{y}_{ij} denote the scaled experimental
 500 observations and simulation outputs (fold-change; protein normalized by control value
 501 directly before ATRA addition) at time i from protein j , where T_j denoted the number of
 502 time points for data set j . Lastly, the third term of the objective function measured the
 503 difference in the *shape* of the measured and simulated protein levels. The scaled value
 504 $0 \leq \mathcal{M}'_{ij} \leq 1$ was given by:

$$\hat{\mathcal{M}}_{ij} = \left(\mathcal{M}_{ij} - \min_i \mathcal{M}_{ij} \right) / \left(\max_i \mathcal{M}_{ij} - \min_i \mathcal{M}_{ij} \right) \quad (14)$$

505 where $\mathcal{M}'_{ij} = 0$ and $\mathcal{M}'_{ij} = 1$ describe the lowest (highest) intensity bands. A similar
 506 scaling was used for the simulation output. We minimized the total model residual $\sum_j E_j$
 507 using a heuristic direct-search optimization procedure, subject to box constraints on the
 508 parameter values, starting from a random initial parameter guess. Each downhill step was
 509 archived and used for ensemble calculations. The optimization procedure (a covariance
 510 matrix adaptation evolution strategy) has been reported previously (55).

511 *Estimation of an effective cell cycle arrest model.* We formulated an effective N-order
 512 polynomial model of the fraction of cells undergoing ATRA-induced cell cycle arrest at
 513 time t , $\hat{\mathcal{A}}(t)$, as:

$$\hat{\mathcal{A}}(t) \simeq a_0 + \sum_{i=1}^{N-1} a_i \phi_i(\mathbf{p}(t), t) \quad (15)$$

514 where a_i were unknown parameters, and $\phi_i(\mathbf{p}(t), t)$ denotes a basis function. The basis
 515 functions were dependent upon the system state; in this study, we assumed $N = 4$ and
 516 basis functions of the form:

$$\phi_i(\mathbf{p}(t), t) = \left(\frac{t}{T} + \frac{p21}{E2F} \Big|_t \right)^{(i-1)} \quad (16)$$

517 The parameters a_0, \dots, a_3 were estimated directly from cell-cycle measurements (biologi-
518 cal replicates) using least-squares.

519 *Availability of model code.* The signaling and gene expression model equations, and the
520 parameter estimation procedure, were implemented in the Julia programming language.
521 The model equations were solved using the ODE23s routine of the ODE package (56). The
522 model code and parameter ensemble is freely available under an MIT software license
523 and can be downloaded from <http://www.varnerlab.org>.

524 *Cell culture and treatment* Human myeloblastic leukemia cells (HL-60 cells) were grown
525 in a humidified atmosphere of 5% CO₂ at 37°C and maintained in RPMI 1640 from Gibco
526 (Carlsbad, CA) supplemented with 5% heat inactivated fetal bovine serum from Hyclone
527 (Logan, UT) and 1× antibiotic/antimicotic (Gibco, Carlsbad, CA). Cells were cultured in
528 constant exponential growth (57). Experimental cultures were initiated at 0.1×10^6 cells/mL
529 24 hr prior to ATRA treatment; if indicated, cells were also treated with GW5074 (2 μ M) 18
530 hr before ATRA treatment. For the cell culture washout experiments, cells were treated
531 with ATRA for 24 hr, washed 3x with prewarmed serum supplemented culture medium
532 to remove ATRA, and reseeded in ATRA-free media as described. Western blot analysis
533 was performed at incremental time points after removal of ATRA.

534 *Chemicals* All-Trans Retinoic Acid (ATRA) from Sigma-Aldrich (St. Louis, MO) was dis-
535 solved in 100% ethanol with a stock concentration of 5mM, and used at a final concen-
536 tration of 1 μ M (unless otherwise noted). The cRaf inhibitor GW5074 from Sigma-Aldrich
537 (St. Louis, MO) was dissolved in DMSO with a stock concentration of 10mM, and used
538 at a final concentration of 2 μ M. HL-60 cells were treated with 2 μ M GW5074 with or with-
539 out ATRA (1 μ M) at 0 hr. This GW5074 dosage had a negligible effect on the cell cycle
540 distribution, compared to ATRA treatment alone.

541 *Immunoprecipitation and western blotting* Approximately 1.2×10^7 cells were lysed using
542 $400\mu\text{L}$ of M-Per lysis buffer from Thermo Scientific (Waltham, MA). Lysates were cleared
543 by centrifugation at $16,950 \times g$ in a micro-centrifuge for 20 min at 4°C . Lysates were
544 pre-cleared using $100\mu\text{L}$ protein A/G Plus agarose beads from Santa Cruz Biotechnology
545 (Santa Cruz, CA) by inverting overnight at 4°C . Beads were cleared by centrifugation and
546 total protein concentration was determined by a BCA assay (Thermo Scientific, Waltham,
547 MA). Immunoprecipitations were setup by bringing lysate to a concentration of 1g/L in a
548 total volume of $300\mu\text{L}$ (M-Per buffer was used for dilution). The anti-Raf antibody was
549 added at $3\mu\text{L}$. A negative control with no bait protein was also used to exclude the di-
550 rect interaction of proteins with the A/G beads. After 1 hr of inversion at 4°C , $20\mu\text{L}$ of
551 agarose beads was added and samples were left to invert overnight at 4°C . Samples
552 were then washed three times with M-Per buffer by centrifugation. Finally proteins were
553 eluted from agarose beads using a laemmli loading buffer. Eluted proteins were resolved
554 by SDS-PAGE and Western blotting. Total lysate samples were normalized by total protein
555 concentration ($20\mu\text{g}$ per sample) and resolved by SDS-PAGE and Western blotting. Sec-
556 ondary HRP bound antibody was used for visualization. All antibodies were purchased
557 from Cell Signaling (Boston, MA) with the exception of α -p621 Raf which was purchased
558 from Biosource/Invitrogen (Carlsbad, CA), and α -CK2 from BD Biosciences (San Jose,
559 CA).

560 *Morphology assessment* Untreated and ATRA-treated HL-60 cells were collected after
561 72 hr and cytocentrifuged for 3 min at 700 rpm onto glass slides. Slides were air-dried
562 and stained with Wright's stain. Slide images were captured at 40X (Leica DM LB 100T
563 microscope, Leica Microsystems).

564 **Competing interests**

565 The authors declare that they have no competing interests.

566 **Author's contributions**

567 J.V and A.Y directed the study. R.T, H.J, R.B and J.C conducted the cell culture measure-
568 ments. J.V, R.B, W.D, K.R and A.S developed the reduced order HL-60 models and the
569 parameter ensemble. W.D and J.V analyzed the model ensemble, and generated figures
570 for the manuscript. The manuscript was prepared and edited for publication by W.D, A.Y
571 and J.V.

572 **Acknowledgements**

573 We gratefully acknowledge the suggestions from the anonymous reviewers to improve
574 this manuscript.

575 **Funding**

576 We acknowledge the financial support to J.V. by the National Science Foundation CA-
577 REER (CBET-0846876) for the support of R.T. and H.J. In addition, we acknowledge
578 support to A.Y. from the National Institutes of Health (CA 30555, CA152870) and a grant
579 from New York State Stem Cell Science. Lastly, we acknowledge the financial support to
580 J.V. and A.Y. from the National Cancer Institute (#U54 CA143876). The content is solely
581 the responsibility of the authors and does not necessarily represent the official views of
582 the National Cancer Institute or the National Institutes of Health.

583 **References**

- 584 1. Bushue N, Wan YJY (2010) Retinoid pathway and cancer therapeutics. *Adv Drug
585 Deliv Rev* 62: 1285-98.
- 586 2. Tang XH, Gudas LJ (2011) Retinoids, retinoic acid receptors, and cancer. *Annu Rev
587 Pathol* 6: 345-64.
- 588 3. Cheung FSG, Lovicu FJ, Reichardt JKV (2012) Current progress in using vitamin d
589 and its analogs for cancer prevention and treatment. *Expert Rev Anticancer Ther*
590 12: 811-37.
- 591 4. Nilsson B (1984) Probable in vivo induction of differentiation by retinoic acid of
592 promyelocytes in acute promyelocytic leukaemia. *Br J Haematol* 57: 365-71.
- 593 5. Warrell RP Jr (1993) Retinoid resistance in acute promyelocytic leukemia: new
594 mechanisms, strategies, and implications. *Blood* 82: 1949-53.
- 595 6. Freemantle SJ, Spinella MJ, Dmitrovsky E (2003) Retinoids in cancer therapy and
596 chemoprevention: promise meets resistance. *Oncogene* 22: 7305-15.
- 597 7. Breitman TR, Selonick SE, Collins SJ (1980) Induction of differentiation of the hu-
598 man promyelocytic leukemia cell line (HL-60) by retinoic acid. *Proc Natl Acad Sci U
599 S A* 77: 2936–2940.
- 600 8. Yen A, Roberson MS, Varvayanis S, Lee AT (1998) Retinoic acid induced
601 mitogen-activated protein (MAP)/extracellular signal-regulated kinase (ERK) kinase-
602 dependent MAP kinase activation needed to elicit HL-60 cell differentiation and
603 growth arrest. *Cancer Res* 58: 3163–3172.
- 604 9. Hong HY, Varvayanis S, Yen A (2001) Retinoic acid causes MEK-dependent RAF
605 phosphorylation through RARalpha plus RXR activation in HL-60 cells. *Differentia-
606 tion* 68: 55–66.
- 607 10. Mangelsdorf DJ, Ong ES, Dyck JA, Evans RM (1990) Nuclear receptor that identifies
608 a novel retinoic acid response pathway. *Nature* 345: 224–229.

- 609 11. Congleton J, MacDonald R, Yen A (2012) Src inhibitors, PP2 and dasatinib, increase
610 retinoic acid-induced association of Lyn and c-Raf (S259) and enhance MAPK-
611 dependent differentiation of myeloid leukemia cells. Leukemia 26: 1180-8.
- 612 12. Shen M, Bunaci R, Congleton J, Jensen H, Sayam L, et al. (2011) Interferon regu-
613 latory factor-1 binds c-Cbl, enhances mitogen activated protein kinase signaling and
614 promotes retinoic acid-induced differentiation of HL-60 human myelo-monoblastic
615 leukemia cells. Leuk Lymphoma 52: 2372-9.
- 616 13. Shen M, Yen A (2009) c-Cbl tyrosine kinase-binding domain mutant G306E abol-
617 ishes the interaction of c-Cbl with CD38 and fails to promote retinoic acid-induced
618 cell differentiation and G0 arrest. J Biol Chem 284: 25664–25677.
- 619 14. Yen A, Varvayanis S, Smith J, Lamkin T (2006) Retinoic acid induces expression of
620 SLP-76: expression with c-FMS enhances ERK activation and retinoic acid-induced
621 differentiation/G0 arrest of HL-60 cells. Eur J Cell Biol 85: 117–132.
- 622 15. Marchisio M, Bertagnolo V, Colamussi ML, Capitani S, Neri LM (1998) Phos-
623 phatidylinositol 3-kinase in HL-60 nuclei is bound to the nuclear matrix and increases
624 during granulocytic differentiation. Biochem Biophys Res Commun 253: 346-51.
- 625 16. Congleton J, Jiang H, Malavasi F, Lin H, Yen A (2011) ATRA-induced HL-60 myeloid
626 leukemia cell differentiation depends on the CD38 cytosolic tail needed for mem-
627 brane localization, but CD38 enzymatic activity is unnecessary. Exp Cell Res 317:
628 910–919.
- 629 17. Wang J, Yen A (2004) A novel retinoic acid-responsive element regulates retinoic
630 acid induced BLR1 expression. Mol Cell Biol 24: 2423 - 2443.
- 631 18. Yen A (1990) HL-60 cells as a model of growth and differentiation: the significance
632 of variant cells. Hematology Review 4: 5-46.
- 633 19. Yang T, Xiong Q, Enslen H, Davis R, Chow CW (2002) Phosphorylation of NFATc4
634 by p38 mitogen-activated protein kinases. Mol Cell Biol 22: 3892–3904.

- 635 20. Wang J, Yen A (2008) A MAPK-positive Feedback Mechanism for BLR1 Signaling
636 Propels Retinoic Acid-triggered Differentiation and Cell Cycle Arrest. *J Biol Chem*
637 283: 4375–4386.
- 638 21. Tasseff R, Nayak S, Song S, Yen A, Varner J (2011) Modeling and analysis of retinoic
639 acid induced differentiation of uncommitted precursor cells. *Integr Biol* 3: 578 - 591.
- 640 22. Jensen HA, Styskal LE, Tasseff R, Bunaciu RP, Congleton J, et al. (2013) The
641 src-family kinase inhibitor pp2 rescues inducible differentiation events in emergent
642 retinoic acid-resistant myeloblastic leukemia cells. *PLoS One* 8: e58621.
- 643 23. Jensen HA, Bunaciu RP, Ibabao CN, Myers R, Varner JD, et al. (2014) Retinoic acid
644 therapy resistance progresses from unilineage to bilineage in hl-60 leukemic blasts.
645 *PLoS One* 9: e98929.
- 646 24. Jensen HA, Bunaciu RP, Varner JD, Yen A (2015) Gw5074 and pp2 kinase inhibitors
647 implicate nontraditional c-raf and lyn function as drivers of retinoic acid-induced mat-
648 uration. *Cell Signal* 27: 1666-75.
- 649 25. Jensen HA, Yourish HB, Bunaciu RP, Varner JD, Yen A (2015) Induced myelomono-
650 cytic differentiation in leukemia cells is accompanied by noncanonical transcription
651 factor expression. *FEBS Open Bio* 5: 789-800.
- 652 26. Milo R, Jorgensen P, Moran U, Weber G, Springer M (2010) Bionumbers—the
653 database of key numbers in molecular and cell biology. *Nucleic Acids Res* 38: D750-
654 3.
- 655 27. Katagiri K, Hattori S, Nakamura S, Yamamoto T, Yoshida T, et al. (1994) Activation
656 of ras and formation of gap complex during tpa-induced monocytic differentiation of
657 hl-60 cells. *Blood* 84: 1780–1789.
- 658 28. Miranda MB, Johnson DE (2007) Signal transduction pathways that contribute to
659 myeloid differentiation. *Leukemia* 21: 1363–1377.
- 660 29. Hickstein DD, Back AL, Collins SJ (1989) Regulation of expression of the cd11b and

- 661 cd18 subunits of the neutrophil adherence receptor during human myeloid differen-
662 tiation. *J Biol Chem* 264: 21812–21817.
- 663 30. Hornstein I, Alcover A, Katzav S (2004) Vav proteins, masters of the world of cy-
664 toskeleton organization. *Cell Signal* 16: 1-11.
- 665 31. Ferrell J (2002) Self-perpetuating states in signal transduction: positive feedback,
666 double-negative feedback and bistability. *Curr Opin Cell Biol* 14: 140-8.
- 667 32. Laslo P, Spooner CJ, Warmflash A, Lancki DW, Lee HJ, et al. (2006) Multilineage
668 transcriptional priming and determination of alternate hematopoietic cell fates. *Cell*
669 126: 755-66.
- 670 33. Xiong W, Ferrell J (2003) A positive-feedback-based bistable 'memory module' that
671 governs a cell fate decision. *Nature* 426: 460-5.
- 672 34. Bagci EZ, Vodovotz Y, Billiar TR, Ermentrout GB, Bahar I (2006) Bistability in apop-
673 tosis: roles of bax, bcl-2, and mitochondrial permeability transition pores. *Biophys J*
674 90: 1546-59.
- 675 35. Luan D, Zai M, Varner JD (2007) Computationally derived points of fragility of a
676 human cascade are consistent with current therapeutic strategies. *PLoS Comput*
677 *Biol* 3: e142.
- 678 36. Friedman AD (2007) Transcriptional control of granulocyte and monocyte develop-
679 ment. *Oncogene* 26: 6816-28.
- 680 37. Dahl R, Walsh JC, Lancki D, Laslo P, Iyer SR, et al. (2003) Regulation of macrophage
681 and neutrophil cell fates by the PU.1:C/EBPalpha ratio and granulocyte colony-
682 stimulating factor. *Nat Immunol* 4: 1029-36.
- 683 38. El-Benna J, Dang PMC, Gougerot-Pocidalo MA, Marie JC, Braut-Boucher F (2009)
684 p47phox, the phagocyte nadph oxidase/nox2 organizer: structure, phosphorylation
685 and implication in diseases. *Exp Mol Med* 41: 217-25.
- 686 39. Hock H, Hamblen MJ, Rooke HM, Traver D, Bronson RT, et al. (2003) Intrinsic re-

- 687 quirement for zinc finger transcription factor gfi-1 in neutrophil differentiation. Immuno-
688 nity 18: 109-20.
- 689 40. Cleghon V, Morrison DK (1994) Raf-1 interacts with fyn and src in a non-
690 phosphotyrosine-dependent manner. *J Biol Chem* 269: 17749–17755.
- 691 41. Zimmermann S, Moelling K (1999) Phosphorylation and regulation of raf by akt (pro-
692 tein kinase b). *Science* 286: 1741–1744.
- 693 42. Ritt DA, Zhou M, Conrads TP, Veenstra TD, Copeland TD, et al. (2007) Ck2 is a
694 component of the ksr1 scaffold complex that contributes to raf kinase activation.
695 *Curr Biol* 17: 179–184.
- 696 43. Hekman M, Wiese S, Metz R, Albert S, Troppmair J, et al. (2004) Dynamic changes
697 in c-raf phosphorylation and 14-3-3 protein binding in response to growth factor stim-
698 ulation: differential roles of 14-3-3 protein binding sites. *J Biol Chem* 279: 14074–
699 14086.
- 700 44. Dhillon AS, Yip YY, Grindlay GJ, Pakay JL, Dangers M, et al. (2009) The c-terminus
701 of raf-1 acts as a 14-3-3-dependent activation switch. *Cell Signal* 21: 1645–1651.
- 702 45. Song JS, Gomez J, Stancato LF, Rivera J (1996) Association of a p95 vav-containing
703 signaling complex with the fcepsilonlonri gamma chain in the rbl-2h3 mast cell line.
704 evidence for a constitutive in vivo association of vav with grb2, raf-1, and erk2 in an
705 active complex. *J Biol Chem* 271: 26962–26970.
- 706 46. Costello PS, Walters AE, Mee PJ, Turner M, Reynolds LF, et al. (1999) The rho-
707 family gtp exchange factor vav is a critical transducer of t cell receptor signals to the
708 calcium, erk, and nf-kappab pathways. *Proc Natl Acad Sci U S A* 96: 3035–3040.
- 709 47. Graham D, Robertson C, Bautista J, Mascarenhas F, Diacovo M, et al. (2007)
710 Neutrophil-mediated oxidative burst and host defense are controlled by a Vav-
711 PLCgamma2 signaling axis in mice. *J Clin Invest* 117: 3445–3452.
- 712 48. Kim HS, Lim IK (2009) Phosphorylated extracellular signal-regulated protein kinases

- 713 1 and 2 phosphorylate sp1 on serine 59 and regulate cellular senescence via tran-
714 scription of p21sdi1/cip1/waf1. *J Biol Chem* 284: 15475–15486.
- 715 49. Milanini-Mongiat J, Pouyss?gur J, Pag?s G (2002) Identification of two sp1 phos-
716 phorylation sites for p42/p44 mitogen-activated protein kinases: their implication in
717 vascular endothelial growth factor gene transcription. *J Biol Chem* 277: 20631–
718 20639.
- 719 50. Zhang Y, Cho YY, Petersen BL, Zhu F, Dong Z (2004) Evidence of stat1 phosphory-
720 lation modulated by mapks, mek1 and msk1. *Carcinogenesis* 25: 1165–1175.
- 721 51. Li Z, Theus MH, Wei L (2006) Role of erk 1/2 signaling in neuronal differentiation of
722 cultured embryonic stem cells. *Dev Growth Differ* 48: 513–523.
- 723 52. Yen A, Reece SL, Albright KL (1984) Dependence of hl-60 myeloid cell differentiation
724 on continuous and split retinoic acid exposures: precommitment memory associated
725 with altered nuclear structure. *J Cell Physiol* 118: 277–286.
- 726 53. Moon TS, Lou C, Tamsir A, Stanton BC, Voigt CA (2012) Genetic programs con-
727 structed from layered logic gates in single cells. *Nature* 491: 249-53.
- 728 54. Wayman JA, Sagar A, Varner JD (2015) Dynamic modeling of cell-free biochemical
729 networks using effective kinetic models. *Processes* 3: 138.
- 730 55. Igel C, Hansen N, Roth S (2007) Covariance matrix adaptation for multi-objective
731 optimization. *Evol Comput* 15: 1-28.
- 732 56. Bezanson J, Edelman A, Karpinski S, Shah VB (2014) Julia: A fresh approach to
733 numerical computing. *CoRR* abs/1411.1607.
- 734 57. Brooks SC, Kazmer S, Levin AA, Yen A (1996) Myeloid differentiation and retinoblas-
735 toma phosphorylation changes in HL-60 cells induced by retinoic acid receptor- and
736 retinoid X receptor-selective retinoic acid analogs. *Blood* 87: 227–237.
- 737 58. Rishi AK, Gerald TM, Shao ZM, Li XS, Baumann RG, et al. (1996) Regulation of the
738 human retinoic acid receptor alpha gene in the estrogen receptor negative human

- 739 breast carcinoma cell lines skbr-3 and mda-mb-435. Cancer Res 56: 5246-52.
- 740 59. Mueller BU, Pabst T, Fos J, Petkovic V, Fey MF, et al. (2006) Atra resolves the dif-
741 ferentiation block in t(15;17) acute myeloid leukemia by restoring pu.1 expression.
742 Blood 107: 3330-8.
- 743 60. Luo XM, Ross AC (2006) Retinoic acid exerts dual regulatory actions on the ex-
744 pression and nuclear localization of interferon regulatory factor-1. Exp Biol Med
745 (Maywood) 231: 619-31.
- 746 61. Sylvester I, Schöler HR (1994) Regulation of the oct-4 gene by nuclear receptors.
747 Nucleic Acids Res 22: 901-11.
- 748 62. Drach J, McQueen T, Engel H, Andreeff M, Robertson KA, et al. (1994) Retinoic
749 acid-induced expression of cd38 antigen in myeloid cells is mediated through
750 retinoic acid receptor-alpha. Cancer Res 54: 1746-52.
- 751 63. Liu M, Iavarone A, Freedman LP (1996) Transcriptional activation of the human
752 p21(waf1/cip1) gene by retinoic acid receptor. correlation with retinoid induction of
753 u937 cell differentiation. J Biol Chem 271: 31723-8.
- 754 64. Bunaciu RP, Yen A (2013) 6-formylindolo (3,2-b)carbazole (ficz) enhances retinoic
755 acid (ra)-induced differentiation of hl-60 myeloblastic leukemia cells. Mol Cancer 12:
756 39.
- 757 65. Balmer JE, Blomhoff R (2002) Gene expression regulation by retinoic acid. J Lipid
758 Res 43: 1773-808.
- 759 66. Rosen ED, Hsu CH, Wang X, Sakai S, Freeman MW, et al. (2002) C/ebpalpha in-
760 duces adipogenesis through ppargamma: a unified pathway. Genes Dev 16: 22-6.
- 761 67. Varley CL, Bacon EJ, Holder JC, Southgate J (2009) Foxa1 and irf-1 intermediary
762 transcriptional regulators of ppargamma-induced urothelial cytodifferentiation. Cell
763 Death Differ 16: 103-14.
- 764 68. Bruemmer D, Yin F, Liu J, Berger JP, Sakai T, et al. (2003) Regulation of the growth

- 765 arrest and dna damage-inducible gene 45 (gadd45) by peroxisome proliferator-
766 activated receptor gamma in vascular smooth muscle cells. Circ Res 93: e38-47.
- 767 69. Delerive P, De Bosscher K, Besnard S, Vanden Berghe W, Peters JM, et al. (1999)
768 Peroxisome proliferator-activated receptor alpha negatively regulates the vascular
769 inflammatory gene response by negative cross-talk with transcription factors nf-
770 kappaB and ap-1. J Biol Chem 274: 32048-54.
- 771 70. Altiok S, Xu M, Spiegelman BM (1997) Ppargamma induces cell cycle withdrawal:
772 inhibition of e2f/dp dna-binding activity via down-regulation of pp2a. Genes Dev 11:
773 1987-98.
- 774 71. Fei J, Cook C, Gillespie M, Yu B, Fullen K, et al. (2011) Atherogenic ω -6 lipids mod-
775 ulate ppar- egr-1 crosstalk in vascular cells. PPAR Res 2011: 753917.
- 776 72. Song EK, Lee YR, Kim YR, Yeom JH, Yoo CH, et al. (2012) Naadp mediates insulin-
777 stimulated glucose uptake and insulin sensitization by ppar γ in adipocytes. Cell Rep
778 2: 1607-19.
- 779 73. Szanto A, Nagy L (2005) Retinoids potentiate peroxisome proliferator-activated re-
780 ceptor gamma action in differentiation, gene expression, and lipid metabolic pro-
781 cesses in developing myeloid cells. Mol Pharmacol 67: 1935-43.
- 782 74. Han S, Sidell N, Fisher PB, Roman J (2004) Up-regulation of p21 gene expres-
783 sion by peroxisome proliferator-activated receptor gamma in human lung carcinoma
784 cells. Clin Cancer Res 10: 1911-9.
- 785 75. Von Knethen A, Brüne B (2002) Activation of peroxisome proliferator-activated re-
786 ceptor gamma by nitric oxide in monocytes/macrophages down-regulates p47phox
787 and attenuates the respiratory burst. J Immunol 169: 2619-26.
- 788 76. Dispirito JR, Fang B, Wang F, Lazar MA (2013) Pruning of the adipocyte peroxisome
789 proliferator-activated receptor γ cistrome by hematopoietic master regulator pu.1.
790 Mol Cell Biol 33: 3354-64.

- 791 77. Chen H, Ray-Gallet D, Zhang P, Hetherington CJ, Gonzalez DA, et al. (1995) Pu.1
792 (spi-1) autoregulates its expression in myeloid cells. *Oncogene* 11: 1549-60.
- 793 78. Steidl U, Rosenbauer F, Verhaak RGW, Gu X, Ebralidze A, et al. (2006) Essential
794 role of jun family transcription factors in pu.1 knockdown-induced leukemic stem
795 cells. *Nat Genet* 38: 1269-77.
- 796 79. Pahl HL, Scheibe RJ, Zhang DE, Chen HM, Galson DL, et al. (1993) The proto-
797 oncogene pu.1 regulates expression of the myeloid-specific cd11b promoter. *J Biol*
798 *Chem* 268: 5014-20.
- 799 80. Yuki H, Ueno S, Tatetsu H, Niiro H, Iino T, et al. (2013) Pu.1 is a potent tumor
800 suppressor in classical hodgkin lymphoma cells. *Blood* 121: 962-70.
- 801 81. Li SL, Schlegel W, Valente AJ, Clark RA (1999) Critical flanking sequences of pu.1
802 binding sites in myeloid-specific promoters. *J Biol Chem* 274: 32453-60.
- 803 82. Timchenko N, Wilson DR, Taylor LR, Abdelsayed S, Wilde M, et al. (1995) Autoreg-
804 ulation of the human c/ebp alpha gene by stimulation of upstream stimulatory factor
805 binding. *Mol Cell Biol* 15: 1192-202.
- 806 83. Lidonnici MR, Audia A, Soliera AR, Prisco M, Ferrari-Amorotti G, et al. (2010) Ex-
807 pression of the transcriptional repressor gfi-1 is regulated by c/ebpalpha and is
808 involved in its proliferation and colony formation-inhibitory effects in p210bcr/abl-
809 expressing cells. *Cancer Res* 70: 7949-59.
- 810 84. D'Alo' F, Johansen LM, Nelson EA, Radomska HS, Evans EK, et al. (2003) The
811 amino terminal and e2f interaction domains are critical for c/ebp alpha-mediated
812 induction of granulopoietic development of hematopoietic cells. *Blood* 102: 3163-
813 71.
- 814 85. Pan Z, Hetherington CJ, Zhang DE (1999) Ccaat/enhancer-binding protein activates
815 the cd14 promoter and mediates transforming growth factor beta signaling in mono-
816 cyte development. *J Biol Chem* 274: 23242-8.

- 817 86. Harris TE, Albrecht JH, Nakanishi M, Darlington GJ (2001) Ccaat/enhancer-binding
818 protein-alpha cooperates with p21 to inhibit cyclin-dependent kinase-2 activity and
819 induces growth arrest independent of dna binding. *J Biol Chem* 276: 29200-9.
- 820 87. Bauvois B, Durant L, Laboureau J, Barthélémy E, Rouillard D, et al. (1999) Upreg-
821 ulation of cd38 gene expression in leukemic b cells by interferon types i and ii. *J*
822 *Interferon Cytokine Res* 19: 1059-66.
- 823 88. Passioura T, Dolnikov A, Shen S, Symonds G (2005) N-ras-induced growth suppres-
824 sion of myeloid cells is mediated by irf-1. *Cancer Res* 65: 797-804.
- 825 89. Dahl R, Iyer SR, Owens KS, Cuylear DD, Simon MC (2007) The transcriptional
826 repressor gfi-1 antagonizes pu.1 activity through protein-protein interaction. *J Biol*
827 *Chem* 282: 6473-83.
- 828 90. Duan Z, Horwitz M (2003) Targets of the transcriptional repressor oncoprotein gfi-1.
829 *Proc Natl Acad Sci U S A* 100: 5932-7.
- 830 91. Chen H, Zhang P, Radomska HS, Hetherington CJ, Zhang DE, et al. (1996) Octamer
831 binding factors and their coactivator can activate the murine pu.1 (spi-1) promoter.
832 *J Biol Chem* 271: 15743-52.
- 833 92. Behre G, Whitmarsh AJ, Coghlan MP, Hoang T, Carpenter CL, et al. (1999) c-jun
834 is a jnk-independent coactivator of the pu.1 transcription factor. *J Biol Chem* 274:
835 4939-46.
- 836 93. Kardassis D, Papakosta P, Pardali K, Moustakas A (1999) c-jun transactivates the
837 promoter of the human p21(waf1/cip1) gene by acting as a superactivator of the
838 ubiquitous transcription factor sp1. *J Biol Chem* 274: 29572-81.
- 839 94. Johnson DG, Ohtani K, Nevins JR (1994) Autoregulatory control of e2f1 expression
840 in response to positive and negative regulators of cell cycle progression. *Genes Dev*
841 8: 1514-25.
- 842 95. Fu M, Zhang J, Lin Y, Zhu X, Ehrengruber MU, et al. (2002) Early growth response

- 843 factor-1 is a critical transcriptional mediator of peroxisome proliferator-activated
844 receptor-gamma 1 gene expression in human aortic smooth muscle cells. J Biol
845 Chem 277: 26808-14.
- 846 96. Mak KS, Funnell APW, Pearson RCM, Crossley M (2011) Pu.1 and haematopoietic
847 cell fate: Dosage matters. Int J Cell Biol 2011: 808524.
- 848 97. Chen F, Wang Q, Wang X, Studzinski GP (2004) Up-regulation of egr1 by 1,25-
849 dihydroxyvitamin d3 contributes to increased expression of p35 activator of cyclin-
850 dependent kinase 5 and consequent onset of the terminal phase of hl60 cell differ-
851 entiation. Cancer Res 64: 5425-33.
- 852 98. Suh J, Jeon YJ, Kim HM, Kang JS, Kaminski NE, et al. (2002) Aryl hydrocarbon
853 receptor-dependent inhibition of ap-1 activity by 2,3,7,8-tetrachlorodibenzo-p-dioxin
854 in activated b cells. Toxicol Appl Pharmacol 181: 116-23.
- 855 99. Shen M, Bunaciu RP, Congleton J, Jensen HA, Sayam LG, et al. (2011) Inter-
856 feron regulatory factor-1 binds c-cbl, enhances mitogen activated protein kinase
857 signaling and promotes retinoic acid-induced differentiation of hl-60 human myelo-
858 monoblastic leukemia cells. Leuk Lymphoma 52: 2372-9.
- 859 100. Bunaciu RP, Yen A (2011) Activation of the aryl hydrocarbon receptor ahr promotes
860 retinoic acid-induced differentiation of myeloblastic leukemia cells by restricting ex-
861 pression of the stem cell transcription factor oct4. Cancer Res 71: 2371-80.
- 862 101. Jackson DA, Pombo A, Iborra F (2000) The balance sheet for transcription: an anal-
863 ysis of nuclear rna metabolism in mammalian cells. FASEB J 14: 242-54.
- 864 102. Zhao ZW, Roy R, Gebhardt JCM, Suter DM, Chapman AR, et al. (2014) Spatial orga-
865 nization of rna polymerase ii inside a mammalian cell nucleus revealed by reflected
866 light-sheet superresolution microscopy. Proc Natl Acad Sci U S A 111: 681-6.
- 867 103. Freitas R, Merkle R (2004) Kinematic Self-Replicating Machines. Oxford University
868 Press.

- 869 104. Yang E, van Nimwegen E, Zavolan M, Rajewsky N, Schroeder M, et al. (2003) Decay rates of human mRNAs: correlation with functional characteristics and sequence
870 attributes. *Genome Res* 13: 1863-72.
- 872 105. Doherty MK, Hammond DE, Clague MJ, Gaskell SJ, Beynon RJ (2009) Turnover
873 of the human proteome: determination of protein intracellular stability by dynamic
874 SILAC. *J Proteome Res* 8: 104-12.
- 875 106. Sehgal PB, Derman E, Molloy GR, Tamm I, Darnell JE (1976) 5,6-dichloro-1-beta-
876 d-ribofuranosylbenzimidazole inhibits initiation of nuclear heterogeneous RNA chains
877 in HeLa cells. *Science* 194: 431-3.
- 878 107. Darzacq X, Shav-Tal Y, de Turris V, Brody Y, Shenoy SM, et al. (2007) In vivo dynamics
879 of RNA polymerase II transcription. *Nat Struct Mol Biol* 14: 796-806.
- 880 108. Kos M, Tollervey D (2010) Yeast pre-rRNA processing and modification occur cotranscriptionally. *Mol Cell* 37: 809-20.
- 882 109. Darnell JE Jr (2013) Reflections on the history of pre-mRNA processing and highlights
883 of current knowledge: a unified picture. *RNA* 19: 443-60.
- 884 110. Boström K, Wettsten M, Borén J, Bondjers G, Wiklund O, et al. (1986) Pulse-chase
885 studies of the synthesis and intracellular transport of apolipoprotein B-100 in Hep G2
886 cells. *J Biol Chem* 261: 13800-6.
- 887 111. Meyers R, editor (2004) *Encyclopedia of Molecular Cell Biology and Molecular
888 Medicine*, Volume 1, 2nd Edition. ISBN: 978-3-527-30543-8. Wiley-Blackwell.
- 889 112. Rosenbluth MJ, Lam WA, Fletcher DA (2006) Force microscopy of nonadherent
890 cells: a comparison of leukemia cell deformability. *Biophys J* 90: 2994-3003.

Table 1: Myelomonocytic transcription factor connectivity used in the signal integration and phenotype modules.

Effector	Effect	Target	Source
RAR α	+	RAR α	(58)
	+	PU.1	(59)
	+	C/EBP α	(36)
	+	IRF-1	(60)
	-	Oct4	(61)
	+	CD38	(62)
	+	p21	(63)
	+	AhR	(64)
	+	Egr-1	(65)
PPAR γ	+	C/EBP α	(66)
	+	IRF-1	(67)
	+	Oct1	(68)
	-	AP-1	(69)
	-	E2F	(70)
	-	Egr-1	(71)
	+	CD38	(72)
	+	CD14	(73)
	+	p21	(74)
	-	p47Phox	(75)
PU.1	-	PPAR γ	(76)
	+	PU.1	(77)
	+	AP-1	(78)
	+	Egr-1	(32)
	+	CD11b	(79)
	+	p21	(80)
	+	p47Phox	(81)
C/EBP α	+	PPAR γ	(66)
	+	PU.1	(37)
	+	C/EBP α	(82)
	+	Gfi-1	(83)
	-	E2F	(84)
	+	CD14	(85)

892

	+	p21	(86)
IRF-1	+	CD38	(87)
	+	p21	(88)
	-	PU.1	(89)
	-	C/EBP α	(90)
	-	E2F	(90)
	-	Egr-1	(32)
	-	p21	(90)
Oct1	+	PU.1	(91)
AP-1	-	PPAR γ	(69)
	+	PU.1	(92)
	+	p21	(93)
E2F	+	E2F	(94)
Egr-1	+	PPAR γ	(95)
	-	Gfi-1	(96)
	+	CD14	(97)
AhR	+	AP-1	(98)
	+	IRF-1	(99)
	-	Oct4	(100)
	-	PU.1	

Table 2: Characteristic model parameters estimated from literature.

Symbol	Description	Value	Units	Source
R_1	RNA polymerase abundance	85,000	copies/cell	(101, 102)
R_2	Ribosome abundance	1×10^6	copies/cell	(103)
G_i	Characteristic gene abundance	2	copies/cell	this study
K_X	Saturation constant transcription	600	copies/cell	this study
K_T	Saturation constant translation	95,000	copies/cell	this study
$t_{1/2,m}$	characteristic mRNA half-life (transcription factor)	2-4	hr	(104)
$t_{1/2,p}$	characteristic protein half-life	10	hr	(105)
$\theta_{m,j}$	characteristic mRNA degradation constant	0.34	hr^{-1}	derived
$\theta_{p,j}$	characteristic protein degradation constant	0.07	hr^{-1}	derived
895				
t_d	HL-60 doubling time	19.5	hr	this study
μ	growth rate	0.035	hr^{-1}	derived
k_d	death rate	0.10μ	hr^{-1}	derived
e_T	elongation rate RNA polymerase	50-100	nt/s	(106–109)
e_X	elongation rate Ribosome	5	aa/s	(110)
$L_{T,o}$	characteristic gene length	15,000	nt	(111)
$L_{X,o}$	characteristic transcript length	5,000	nt	derived
k_T	characteristic transcription rate	1.44	hr^{-1}	derived
k_X	characteristic translation rate	3.60	hr^{-1}	derived
D	Diameter of an HL-60 cell	12.4	μm^3	(112)
f_C	cytoplasmic fraction	0.51	dimensionless	(112)

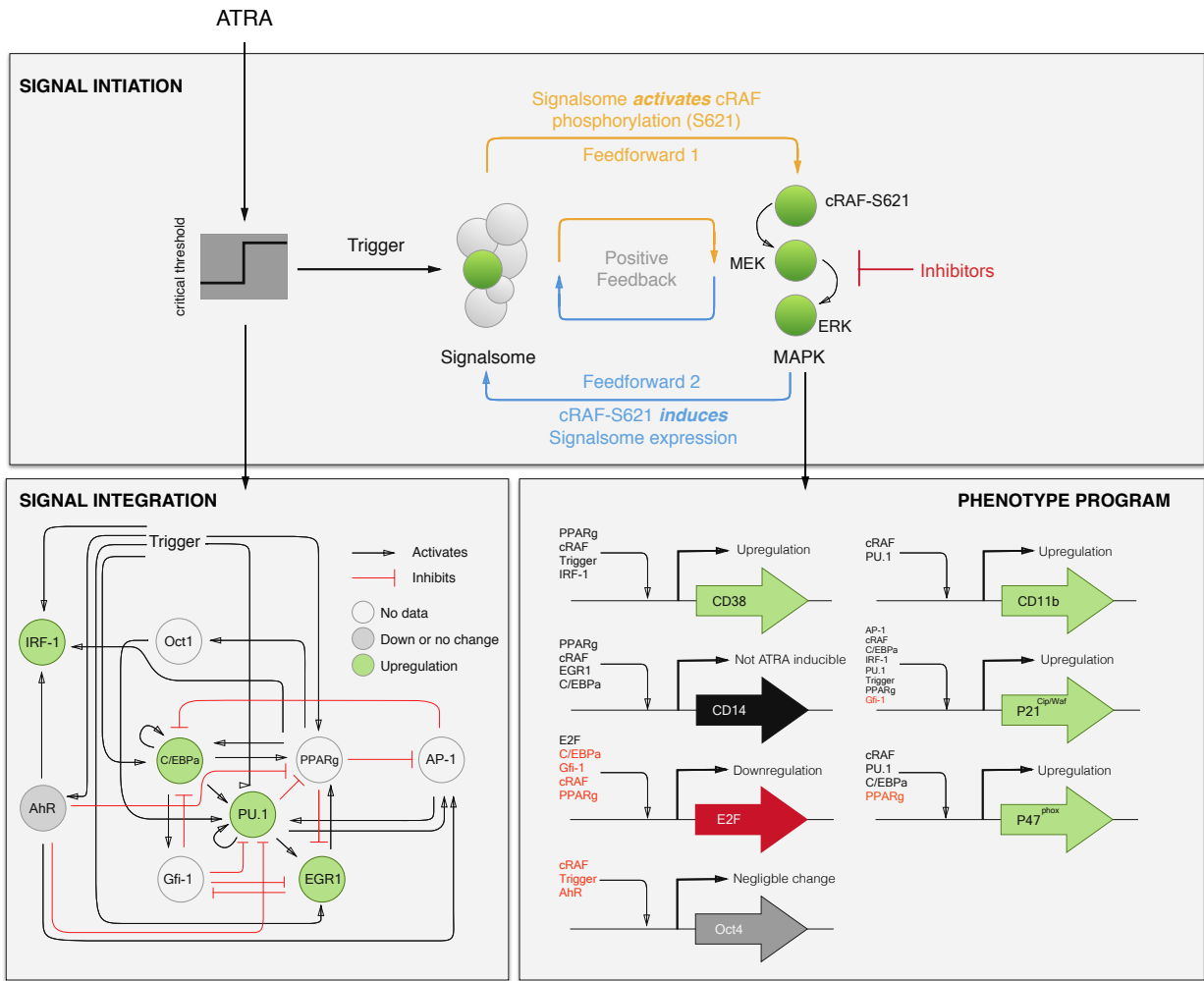


Fig. 1: Schematic of the effective ATRA differentiation circuit. Above a critical threshold, ATRA activates an upstream Trigger, which induces signalsome complex formation. Signalsome activates the mitogen-activated protein kinase (MAPK) cascade which in turn drives the differentiation program and signalsome formation. Both Trigger and activated cRaf-pS621 drive a phenotype gene expression program responsible for differentiation. Trigger activates the expression of a series of transcription factors which in combination with cRaf-pS621 result in phenotypic change.

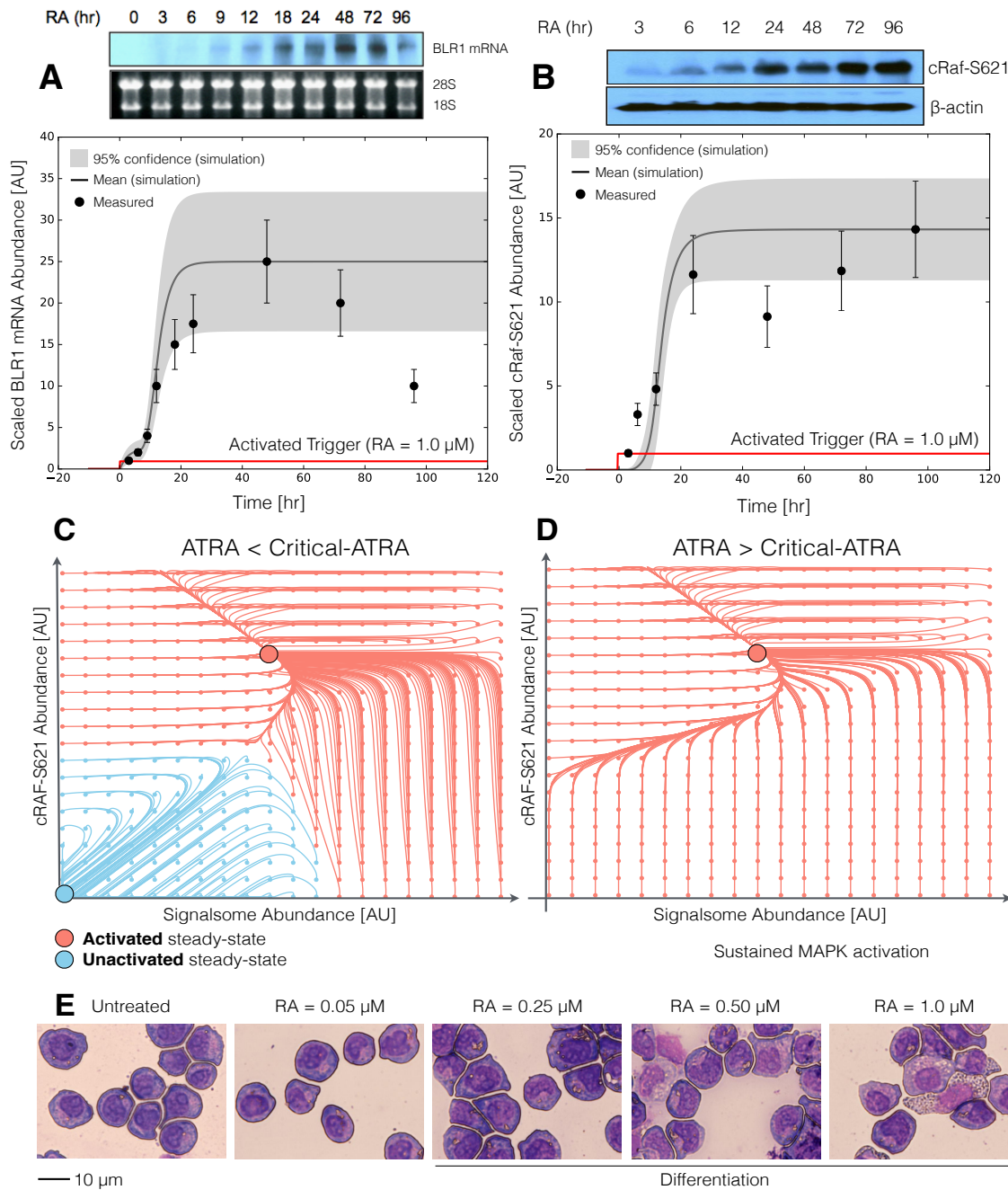


Fig. 2: Model analysis for ATRA-induced HL-60 differentiation. A: BLR1 mRNA versus time following exposure to 1 μ M ATRA at $t = 0$ hr. B: cRaf-pS621 versus time following exposure to 1 μ M ATRA at $t = 0$ hr. Points denote experimental measurements, solid lines denote the mean model performance. Shaded regions denote the 99% confidence interval calculated over the parameter ensemble. C: Signalsome and cRaf-pS621 nullclines for ATRA below the critical threshold. The model had two stable steady states and a single unstable state in this regime. D: Signalsome and cRaf-pS621 nullclines for ATRA above the critical threshold. In this regime the model had only a single stable steady state. E: Morphology of HL-60 as a function of ATRA concentration ($t = 72$ hr).

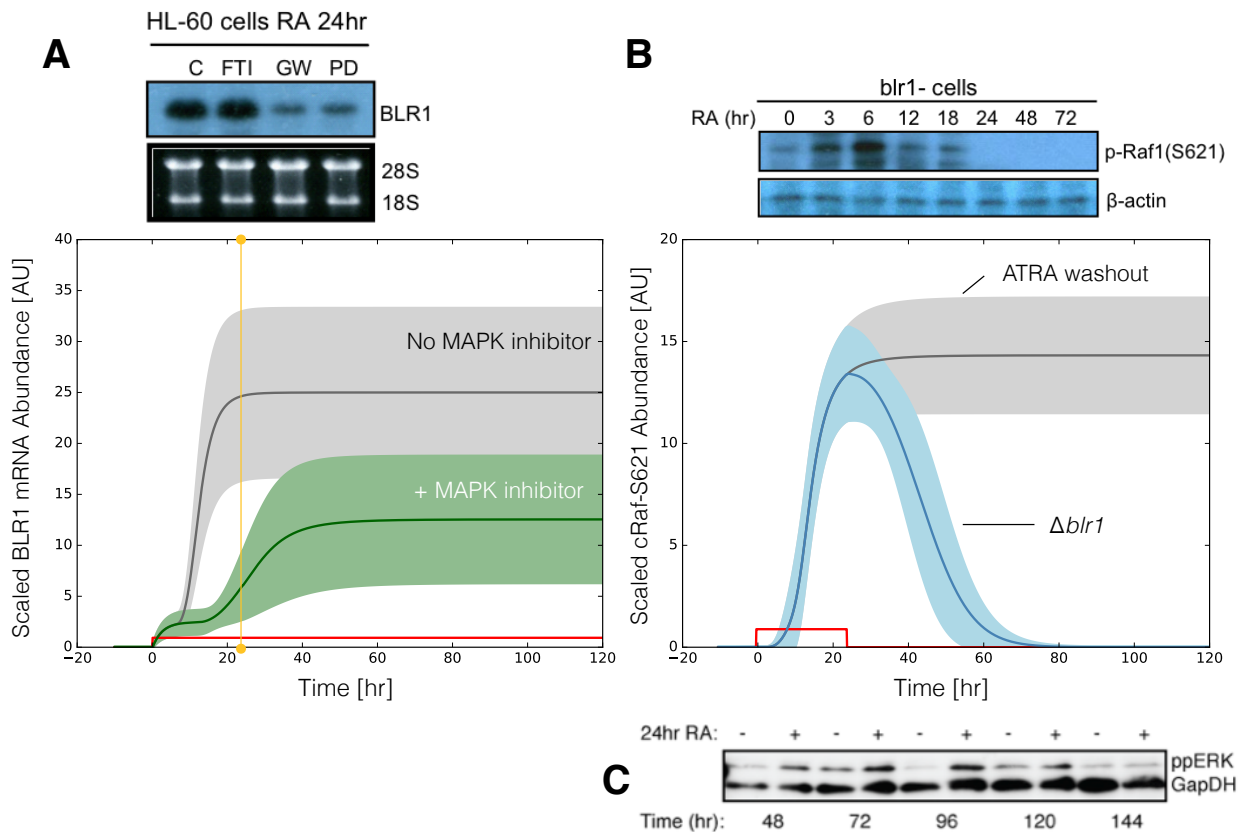


Fig. 3: Model simulation following exposure to $1\mu\text{M}$ ATRA. A: BLR1 mRNA versus time with and without MAPK inhibitor. B: cRaf-pS621 versus time following pulsed exposure to $1\mu\text{M}$ ATRA with and without BLR1. Solid lines denote the mean model performance, while shaded regions denote the 99% confidence interval calculated over the parameter ensemble. C: Western blot analysis of phosphorylated ERK1/2 in ATRA washout experiments. Experimental data in panels A and B were reproduced from Wang and Yen (20), data in panel C is reported in this study.

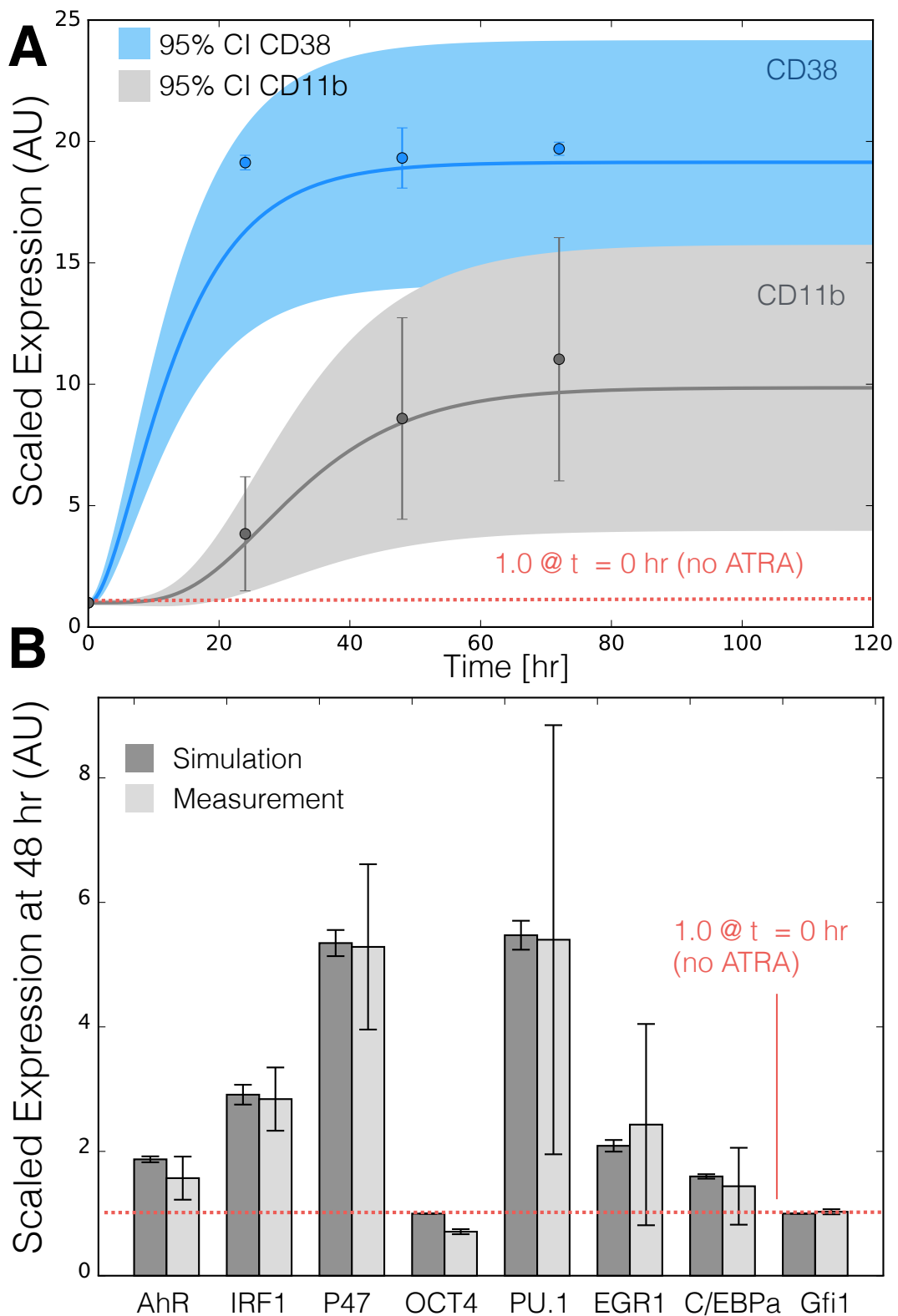


Fig. 4: Model simulation of the HL-60 gene expression program following exposure to $1\mu\text{M}$ ATRA at $t = 0$ hr. A: CD38 and CD11b expression versus time following ATRA exposure at time $t = 0$ hr. B: Gene expression at $t = 48$ hr following ATRA exposure. Experimental data in panels A and B were reproduced from Jensen et al. (25).

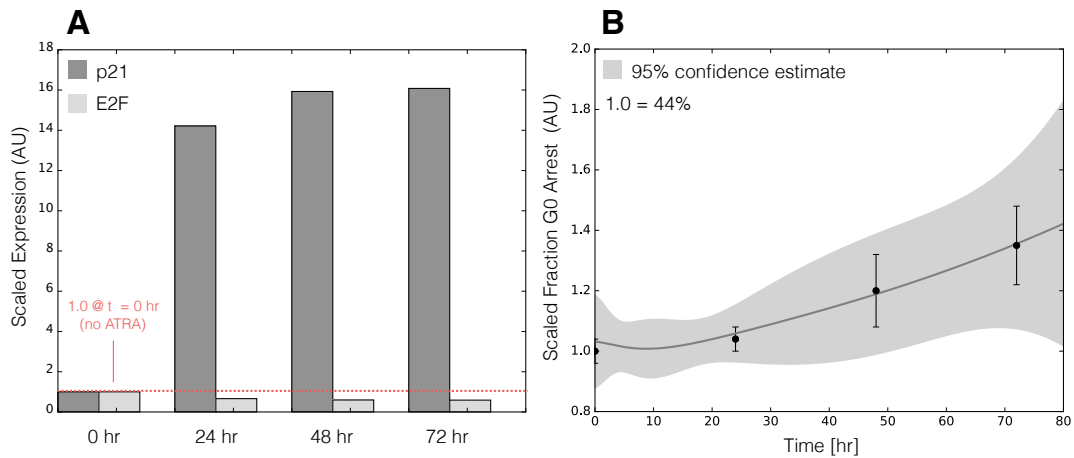


Fig. 5: Model simulation of HL-60 cell-cycle arrest following exposure to $1\mu\text{M}$ ATRA at $t = 0$ hr. A: Predicted p21 and E2F expression levels for the best parameter set following ATRA exposure at time $t = 0$ hr. B: Estimated fraction of HL-60 cells in G0 arrest following ATRA exposure at time $t = 0$ hr. The gray region denotes the 95% confidence estimate of the polynomial model. Experimental data in panel B was reproduced from Jensen et al. (25).

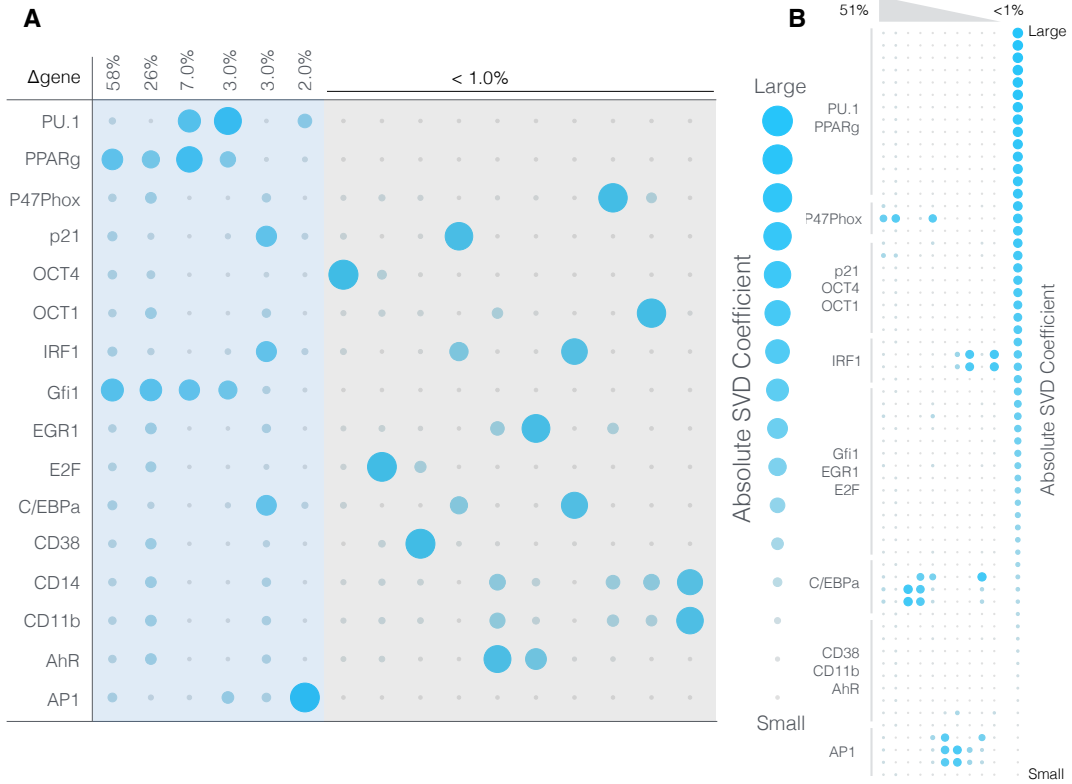


Fig. 6: Robustness of the HL-60 differentiation program following exposure to $1\mu\text{M}$ ATRA at $t = 0$ hr. A: Singular value decomposition of the system response (l^2 -norm between the perturbed and nominal state) following pairwise gene knockout simulations using the best fit parameter set. The percentage at the top of each column describes the fraction of the variance in the system state captured by the node combinations in the rows. B: Singular value decomposition of the system response (l^2 -norm between the perturbed and nominal state) following the pairwise removal of connections.

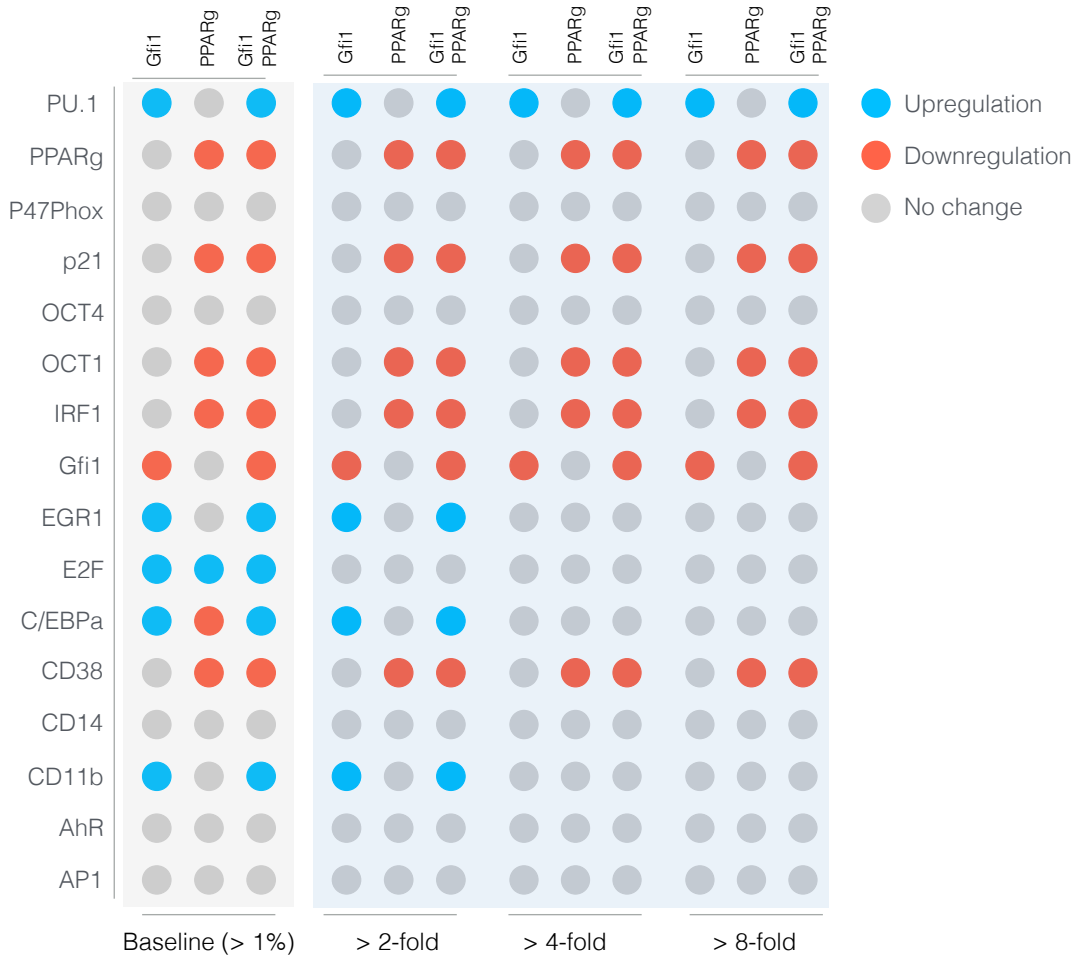


Fig. 7: Robustness of the HL-60 differentiation program following exposure to $1\mu\text{M}$ ATRA at $t = 0$ hr. Protein fold change at $t = 48$ hr (rows) in single and double knock-out mutants (columns) relative to wild-type HL-60 cells. The responses were grouped into $>2,4$ and 8 fold changes. The best fit parameter set was used to calculate the protein fold change.

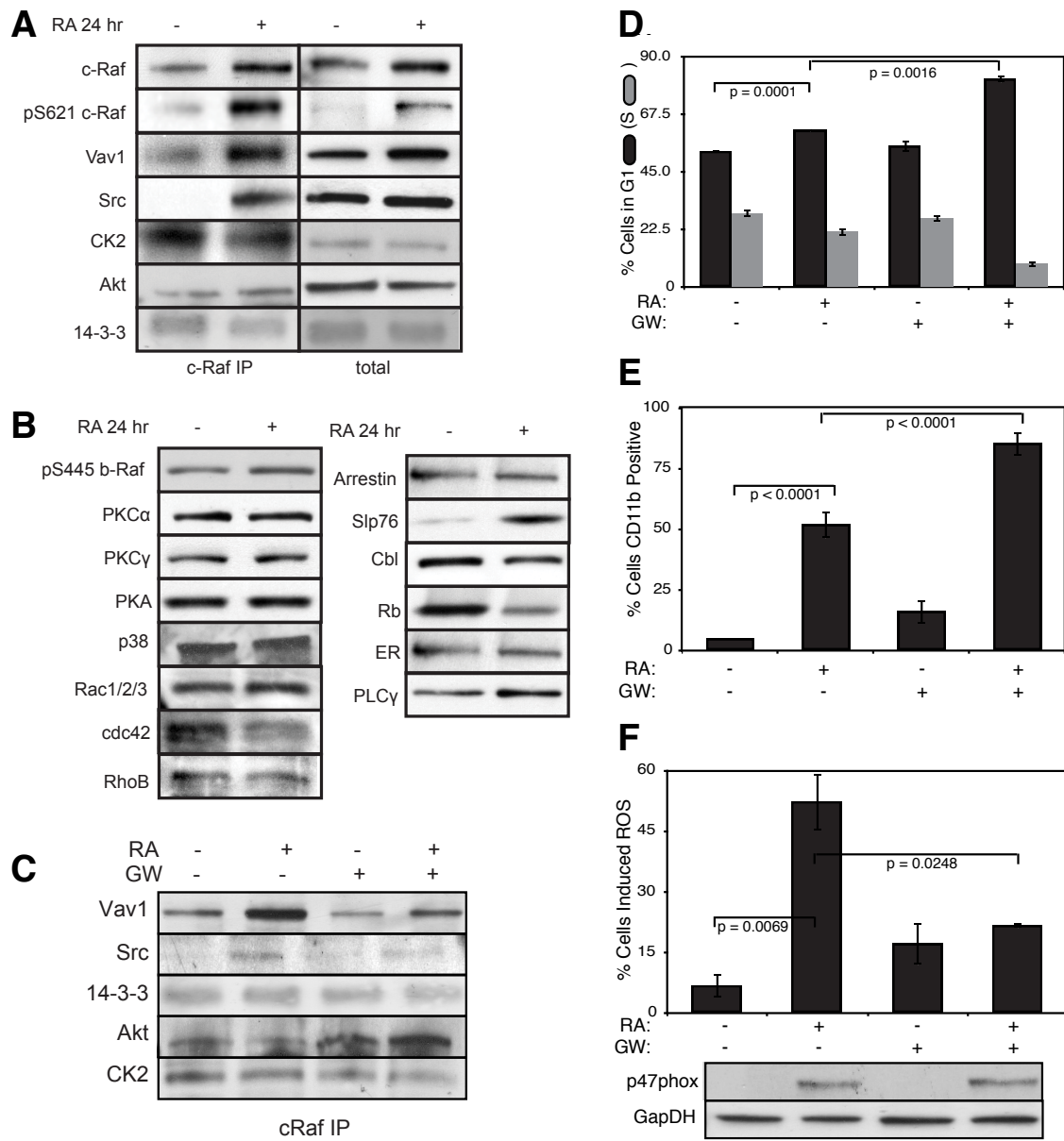


Fig. 8: Investigation of a panel of possible Raf interaction partners in the presence and absence of ATRA. A: Species identified to precipitate out with Raf: first column shows Western blot analysis on total Raf immunoprecipitation with and without 24 hr ATRA treatment and the second on total lysate. B: The expression of species considered that did not precipitate out with Raf at levels detectable by Western blot analysis on total lysate. C: Effect of the Raf inhibitor GW5074 on Raf interactions as determined by Western blot analysis of total Raf immunoprecipitation. The Authors note the signal associated with Src was found to be weak. D: Cell Cycle distribution as determined by flow cytometry indicated arrest induced by ATRA, which was increased by the addition of GW5074. E: Expression of the cell surface marker CD11b as determined by flow cytometry indicated increased expression induced by ATRA, which was enhanced by the addition of GW5074. F: Inducible reactive oxygen species (ROS) as determined by DCF flow cytometry. The functional differentiation response of ATRA treated cells was mitigated by GW5074.